Exploring the Relationship between Glaucoma and Macular Ellipsoid Zone

Doctoral thesis

to obtain a doctorate (Dr. med.)

from the Faculty of Medicine

of the University of Bonn

Ke Lu

from Hubei, China

2026

Written with authorization of
the Faculty of Medicine of the University of Bonn

First reviewer: Prof. Dr. Frank G. Holz

Second reviewer: Prof. Dr. Peter Michael Krawitz

Day of oral examination: 15.01.2026

From the Department of Ophthalmology, University of Bonn

Table of contents

List of abbreviations

ATP	Adenosine Triphosphate
BCVA	Best Corrected Visual Acuity
CI	Confidence Intervals
ELM	External Limiting Membrane
EZ	Ellipsoid Zone
GCL	Ganglion Cell Layer
HVF	Humphrey Visual Field
IOP	Intraocular Pressure
IVZ	inferior vulnerability zone
MD	Mean Deviation
MVZ	Macular Vulnerability Zone
NTG	Normal Tension Glaucoma
OPP	Ocular Perfusion Pressure
POAG	Primary Open-angle Glaucoma
rEZR	relative Ellipsoid Zone Reflectivity
RGCs	Retinal Ganglion Cells
RNFL	Retinal Nerve Fibre Layer
ROI	Region of Interest
RPE	Retinal Pigment Epithelium
RTSD	Retrograde Transsynaptic Degeneration
SD-OCT	spectral-domain Optical Coherence Tomography
SVZ	Superior Vulnerability Zone
TM	Trabecular Meshwork

1. Introduction

Glaucoma, the second leading cause of blindness in the world, is a group of progressive optic neuropathies, which are commonly characterised by the slow progressive degeneration of retinal ganglion cells (RGCs), leading to the excavation or cupping of the optic disc, damage to the optic nerve and corresponding loss of vision (Weinreb and Khaw 2004). Glaucoma affects more than 70 million individuals globally, with approximately 10 % of them being bilaterally blind (Quigley and Broman 2006). The global burden of the disease is expected to increase substantially, with projections indicating that the number of people living with glaucoma will rise to approximately 111.8 million by the year 2040. The estimated prevalence of glaucoma in individuals aged 40 to 80 years is 3.54 % (Tham et al., 2014), underscoring its significance as a major global public health challenge. Early detection, accurate diagnosis, and effective monitoring of disease progression are therefore critical in minimizing visual impairment and improving patient outcomes. While elevated intraocular pressure (IOP) remains the most significant risk factor, glaucomatous damage can occur even in the presence of normal IOP, reflecting the complex and multifactorial pathogenesis of the disease. Other factors such as low intracranial pressure, abnormal structural susceptibility of the lamina cribrosa, abnormal ocular blood flow, autoimmunity, and mitochondrial dysfunction may also be involved (Quigley 2011).

Glaucoma traditionally affects the inner retina and the optic nerve head. However, advances in retinal imaging, particularly optical coherence tomography (OCT), have made it possible to focus on and assess the outer retinal layers in greater detail, especially in the macula region, revealing that the impact of glaucoma may be more widespread than previously believed.

1.1 Subtypes of Glaucoma：POAG and NTG

Glaucoma can be divided into open angle glaucoma and angle closure glaucoma, with primary open angle glaucoma (POAG) being the most common form (Sakurada et al., 2020) and classically defined by the presence of an open anterior chamber angle, characteristic optic nerve damage, visual field defects, and IOP above 21 mmHg. However, a considerable subset of patients develops glaucomatous changes at statistically normal IOP levels (≤ 21 mmHg), a condition termed normal tension glaucoma (NTG).

Although POAG and NTG share similar structural and functional outcomes, their underlying mechanisms appear to differ. POAG is typically linked to pressure-dependent factors, such as mechanical deformation of the lamina cribrosa, disrupted axoplasmic flow, and elevated IOP. In contrast, NTG is associated with pressure-independent mechanisms including vascular dysregulation, impaired ocular blood flow, systemic hypotension, oxidative stress, and mitochondrial dysfunction (Flammer et al., 2002). These differences may influence not only optic nerve head vulnerability but also the extent and pattern of retinal damage, particularly in the macular region.

Clinically, NTG exhibits distinct characteristics compared to POAG. NTG tends to produce more para-central visual field defects (Hood et al., 2013), a higher incidence of peripapillary disc hemorrhages (Drance hemorrhages) (Drance et al., 2001), and is more frequently associated with systemic vascular abnormalities such as migraine, Raynaud’s phenomenon (Barbosa-Breda et al., 2019; Flammer et al., 2002), peripheral vasospasm, and nocturnal dips in systemic blood pressure (Leske et al., 2008). These clinical patterns further support the notion that vascular and metabolic factors, rather than mechanical stress alone, contribute to NTG pathophysiology. Understanding the similarities and differences between these two subtypes is essential for identifying subtype-specific biomarkers and optimizing targeted therapeutic strategies.

1.2 The Important Role of the Macula in Glaucoma Diagnosis and Monitoring

The macula plays a critical role in central vision and is densely populated with RGCs, particularly in the parafoveal region. More than half of all RGCs in the human retina are located within the central 4.5 mm of the macula (Curcio and Allen 1990), making this area highly susceptible to glaucomatous damage. Therefore, the macula is considered a key target for early detection and functional monitoring in glaucoma.

Traditionally, structural assessments in glaucoma have focused on peripapillary retinal nerve fiber layer (RNFL) thickness and optic nerve head morphology. However, the advent of spectral-domain OCT (SD-OCT) has enabled high-resolution, layer-specific imaging, allowing for precise quantification of macular parameters such as the ganglion cell complex and ganglion cell inner plexiform layer. These inner macular layers are now recognized as sensitive and reliable biomarkers of glaucomatous damage, often demonstrating thinning even before detectable RNFL loss (Hood et al., 2013; Mwanza et al., 2011).

1.3 The Ellipsoid Zone: Anatomy and Functional Significance

The ellipsoid zone (EZ), previously known as the inner segment/outer segment junction, appears as a hyperreflective band on SD-OCT and represents the mitochondria-rich ellipsoid portion of the photoreceptor inner segments. The integrity of the EZ is directly related to photoreceptor metabolic activity and function. As such, EZ continuity and reflectivity have been widely used as imaging biomarkers for photoreceptor health and visual acuity outcomes in retinal diseases such as age-related macular degeneration, diabetic macular edema, and inherited retinal dystrophies (Spaide and Curcio 2011).

Disruption or attenuation of the EZ typically indicates photoreceptor dysfunction and is

strongly associated with visual impairment. Given the dense concentration of cones in the foveal region and their high metabolic demand, the EZ is particularly sensitive to diseases that affect cellular respiration or mitochondrial energy production.

1.4 Mitochondrial Dysfunction in Glaucoma and Its Potential Link to EZ Changes

Mitochondria are essential organelles that maintain cellular homeostasis through adenosine triphosphate (ATP) production, calcium regulation, and reactive oxygen species management. In the eye, they are particularly important in high-energy-demanding cells such as RGCs and photoreceptors. Mitochondrial dysfunction has long been implicated in the pathogenesis of glaucoma, especially in subtypes where IOP is not elevated, namely NTG (Duarte 2021; Jeoung et al., 2014; Trivli et al., 2019).

In glaucomatous optic neuropathy, studies have reported reduced mitochondrial DNA copy number, impaired oxidative phosphorylation, and structural abnormalities in mitochondria of RGCs and the optic nerve head (Lee et al., 2011; Osborne and del Olmo-Aguado 2013). Furthermore, emerging evidence suggests that mitochondrial defects are also relevant in POAG. Yang et al. summarized that mitochondrial dysfunction has been observed in multiple ocular tissues affected by glaucoma, including trabecular meshwork (TM) and TM cells, iris, lamina cribrosa cells, optic nerve head, and RGCs (Yang et al., 2013). Abu-Amero et al. also reported a range of mitochondrial abnormalities in POAG patients, implicating oxidative stress and systemic mitochondrial insufficiency as potential contributing factors (Abu-Amero et al., 2006).

Photoreceptors, especially cones in the central macula, depend heavily on mitochondrial function due to their exceptionally high ATP demand for phototransduction. The EZ, representing the photoreceptor inner segments, is rich in mitochondria. Therefore, the

integrity, reflectivity, and thickness of the EZ on OCT may serve as an indirect indicator of photoreceptor mitochondrial health. In NTG, mitochondrial dysfunction and vascular dysregulation are more pronounced, which may make photoreceptors, particularly foveal cones, more susceptible to metabolic stress. This could potentially result in subtle alterations in the EZ.

Although mitochondrial dysfunction in glaucoma has received increasing attention, it remains unclear whether photoreceptors and their associated mitochondrial structures, namely the EZ, are directly affected in glaucomatous eyes. Clarifying this gap is essential, as mitochondrial damage in the outer retina may result from trans-synaptic degeneration or reflect a broader systemic mitochondrial vulnerability (Nork et al., 2000). Investigating EZ changes by different methods may thus offer new insights into macular and outer retinal involvement in glaucoma and contribute to identifying novel imaging biomarkers that distinguish various glaucoma subtypes.

1.5 The Ellipsoid Zone as an Imaging Biomarker: Current Perspectives

Over the past decade, the EZ has emerged as a robust, non-invasive biomarker for photoreceptor integrity in a variety of retinal diseases. Quantitative and qualitative EZ metrics, including reflectivity, thickness, and continuity, have been used to predict visual acuity and monitor treatment responses (Shin et al., 2012). However, most of this work has focused on outer retinal disorders, and the role of the EZ in inner retinal diseases such as glaucoma is only beginning to be explored. Thus, current evidence remains sparse, and no established protocols exist for EZ evaluation in glaucoma. Exploring EZ changes in glaucoma may help reveal outer retinal involvement and provide additional structural markers beyond traditional inner retinal assessments.

1.6 Current Gaps in Knowledge and Rationale for This Study

Despite advances in glaucoma imaging, the extent to which outer retinal structures, particularly the EZ, are involved in glaucoma remains uncertain. While a limited number of studies have investigated EZ changes in glaucomatous eyes, no research to date has directly compared these alterations between POAG and NTG. This represents a significant knowledge gap, especially considering the distinct pathophysiological mechanisms underpinning these subtypes. Given the critical role of mitochondrial function in EZ visibility and the known vascular and metabolic disturbances in NTG, assessing EZ intensity may offer valuable insights into retinal pathology associated with different glaucoma subtypes.

This study aims to investigate whether the mitochondria-rich EZ in the outer retina is affected in glaucoma and to further validate the potential association between glaucomatous pathology and mitochondrial dysfunction. Additionally, it seeks to determine whether such EZ alterations are linked to subtype-specific pathophysiological mechanisms, thereby providing new insights into the identification of novel biomarkers for differentiating glaucoma subtypes.

2. Methods

The study was approved by the ethics committee at the Faculty of Medicine, University of Bonn, and adhered to the tenets of the Declaration of Helsinki. The content and purpose of the study were explained to all participants and written informed consent was obtained for eachrecruited individual.

2.1 Subjects and Study Design

All the subjects, including the POAG and healthy eye volunteers, who visited the glaucoma and retina department at the University Eye Hospital Bonn were enrolled between June 2022 and June 2023. All participants underwent a comprehensive ophthalmologic examination, which included best corrected visual acuity (BCVA), refraction, slit-lamp biomicroscopy, IOP measurement using Goldmann applanation tonometry (Haag-Streit, Koniz, Switzerland), gonioscopy, central corneal thickness (Orbscan 73 II; Bausch & Lomb Surgical, Rochester, New York, USA), central 24-2 threshold testing of the Humphrey Visual Field (HVF) (HFAII, Carl Zeiss Meditec, Inc., Dublin, CA) and SD-OCT (Heidelberg Engineering, Heidelberg, Germany).

For all the NTG eyes, the maximum IOP was always measures as lower than 21mmHg. All eyes with high-pressure glaucoma were defined as POAG if the IOP was above 21 mmHg at any visit. For outcomes with VF defects, both POAG and NTG individuals were classified into three groups: significantly affected group, early glaucoma group and pre-perimetric glaucoma group. Pre-perimetric glaucoma group was defined as eyes with normal VF results and one or more localized RNFL defects on OCT in keeping with the classical structural changes described for glaucoma and confirmed with the finding of a matching glaucomatous disc appearance (sectoral loss of neuro-retinal rim, disc notching, bayonetting, etc.). The other two groups (significantly affected group and early glaucoma

group) exhibited varying degrees of VF defects. These groups were further categorized based on the characteristics of the VF defects into isolated superior hemisphere, isolated inferior hemisphere, both hemispheres, and paracentral involvement, as illustrated in Figure 1. In this study, the classification of participants into the various sub-groups was determined by a glaucoma expert based on the evaluation of their VF test.

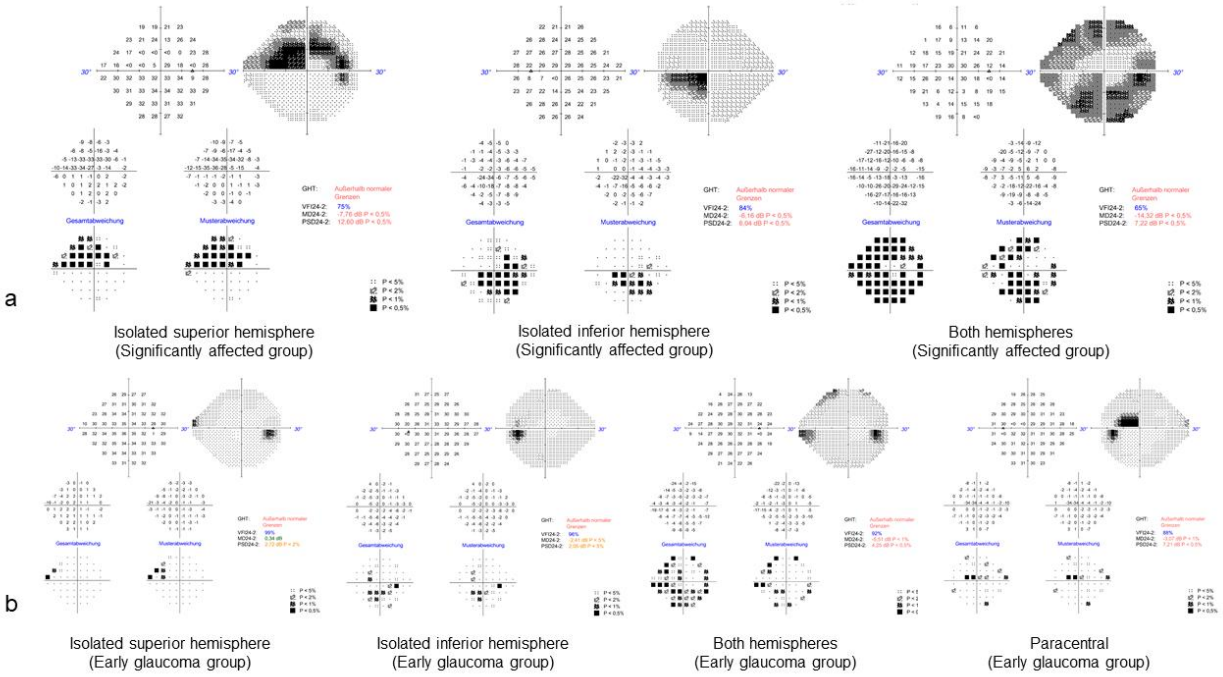

Figure 1: Schematic illustration of the characteristics of visual field defects from our patients. Representative VF defect patterns observed in glaucoma patients included in this study. Patients were categorized into a significantly affected group and an early glaucoma group based on severity. Within the significantly affected group (upper row a), patients were further subdivided into three categories based on the characteristics of their VF defects: Isolated superior hemisphere, Isolated inferior hemisphere, and both hemispheres. Similarly, the early glaucoma group was classified into four categories: Isolated superior hemisphere, Isolated inferior hemisphere, both hemispheres, and paracentral (lower row b).

The Isolated superior hemisphere category was defined as VF defects located exclusively or predominantly in the superior field, while the Isolated inferior hemisphere category referred to defects located exclusively or predominantly in the inferior field. The category with both hemispheres included defects of approximately equal severity in both the superior and inferior fields. Lastly, the Paracentral category was defined by defects in

the paracentral region, characterized by three or more contiguous points with an abnormal probability score of P < 2 % or at least one point with P < 1 %.

The inclusion criteria for the study were as follows: a) Age between 35 and 75 years old; b) BCVA greater than or equal to 20/40 in the Snellen equivalent; c) a spherical refraction greater than - 6 diopters (D) and less than 3 D; d) diagnosed POAG，i) patients with IOP greater than 21mmHg were classified as POAG, ii) patients with IOP lower than 21mmHg were classified as NTG. The exclusion criteria were: a) unwilling or unable to give informed consent; b) a history of intraocular surgery (except uncomplicated cataract surgery); c) history of retinal laser photocoagulation; d) any neurological and/or systemic diseases potentially affecting the retinal structure and/or function; e) no light perception.

Moreover, we performed a stepwise regression analysis using three models to evaluate the association between potential predictors and EZ intensity, progressively adjusting for age, sex, and retinal structural parameters. In Model 1, a univariable regression was conducted to evaluate the unadjusted association between predictors and EZ intensity. Model 2 included age and sex as covariates to control for potential confounding, enabling a clearer evaluation of the effects of the main predictors on EZ intensity. Finally, in Model 3 (+GCL and RNFL adjusted model), we further adjusted for the mean values of ganglion cell layer (GCL) and RNFL to evaluate the combined influence of these biological factors along with the demographic variables. By comparing these three models, we were able to better understand how each factor independently or jointly affects the EZ intensity.

2.2 Imaging protocol and image pre-processing

All measurements were performed by one experienced examiner and acquired in non-mydriatic eyes using a Spectralis HRA+OCT device (Heidelberg Engineering, Heidelberg, Germany) combined with SD-OCT confocal scanning laser ophthalmoscopy

and near-infrared reflectance imaging. In this study, retinal imaging was performed using Posterior Pole Asymmetry Analysis, which consists of 241 B-scans, each composed of 768 A-scans. Scans were performed in high-speed mode with the automatic real time function of 15 frames. The pattern size of volume scan in the central area for each eye was 25° × 30°. Scans were acquired using eye-tracking, and if tracking failed, we manually adjusted the orientation and position of the scan volume so that the latter was centered on the macula, parallel to the mid-axis of the line connecting the macula to the optic disc (Figure 2A). We examined all automatically generated B-scan lines in each retinal image to determine if there were segmentation errors (Figure 2B). If segmentation errors were found, they were corrected manually using the Heidelberg Eye Explorer software (HEYEX, software version 1.10.4.0, Heidelberg Engineering).

2.3 Determination and Analysis of the relative Ellipsoid Zone Reflectivity

The reflectance ratio of the second outer retinal reflective band (green line) to the first (pink line) (Figure 2 B), referred to as the relative Ellipsoid Zone Reflectivity (rEZR), was determined using MatLab (Version 9.5 Natick, The MathWorks, MA, USA). The latter has been widely employed in studies as a biomarker for assessing mitochondrial changes in the retina. In this study, EZ intensity was represented by rEZR. The reflectivity of the ELM is relatively stable across a wide eccentricity range and is less influenced by age or retinal degeneration, making it a reliable reference for rEZR calculations. Figure 3 illustrates an example of a SD-OCT horizontal line scan. Retinal layers were segmented and exported as raw images using the Heyex software (Heidelberg Engineering, Germany), and quantitative analyses of pixel reflectivities were performed on these raw datasets (Figure 3B). The foveal coordinates were identified using ImageJ (Version 1.51j8, Wayne Rasband, National Institutes of Health, USA), and segmentation coordinates of retinal layers, exported as XML files, were superimposed onto the raw images. Subsequently, OCT B-scans were straightened along the coordinates of the

retinal pigment epithelium (RPE) to enable accurate determination of rEZR, even in eyes with significant curvature in the posterior pole (Figure 3C).

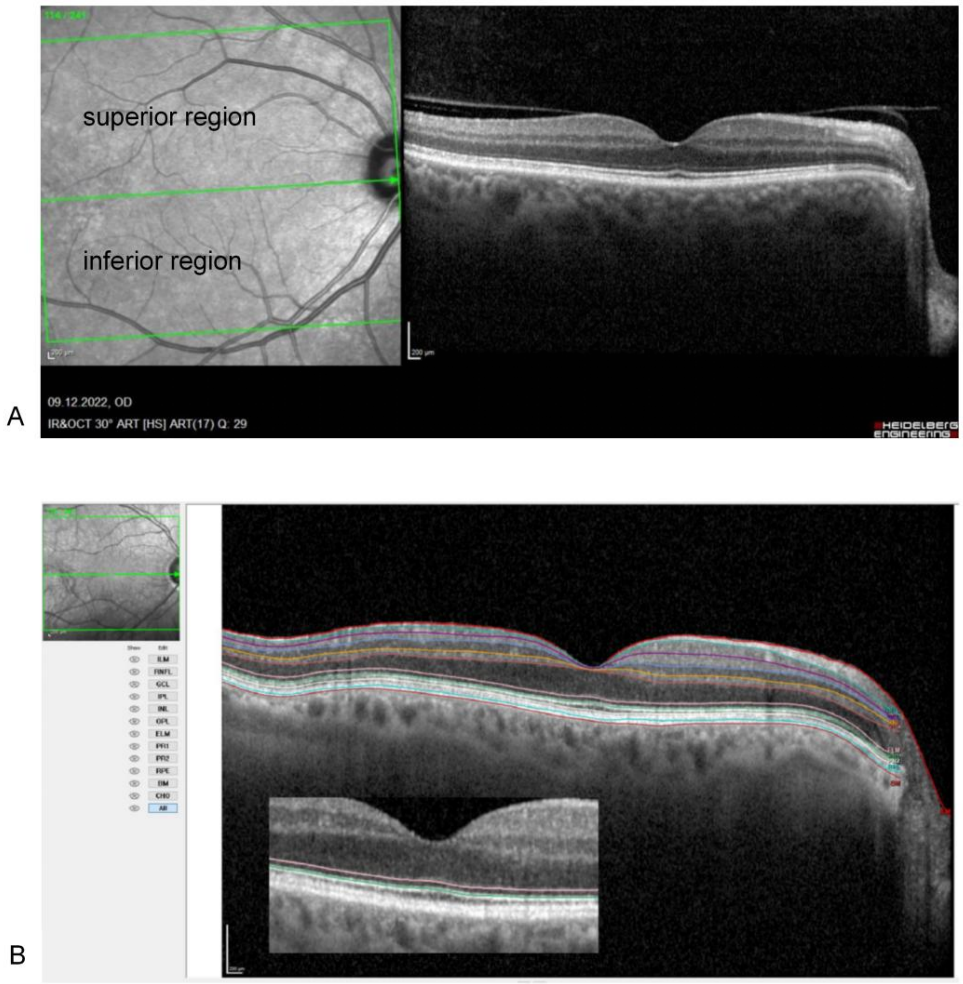

Figure 2: Illustration of SD-OCT Scanning and Retinal Layer Segmentation. (A) An example of near-infrared imaging and an SD-OCT line scan (mid-axis) in logarithmic display. The near-infrared image highlights the scan volume (green box), which is centered on the macula and aligned parallel to the mid-axis connecting the macula and the optic disc. The scan volume comprises a total of 241 B-scans, covering an area of 25° × 30°, corresponding to 768 × 900 pixels in the retinal image. For inter-hemisphere analysis, the scan volume was divided into the superior region and inferior region based on the mid-axis. (B) Correct retinal layer segmentation. The retinal structure is delineated using lines of different colors, with the pink line representing the external limiting membrane (ELM) and the green line representing the EZ.

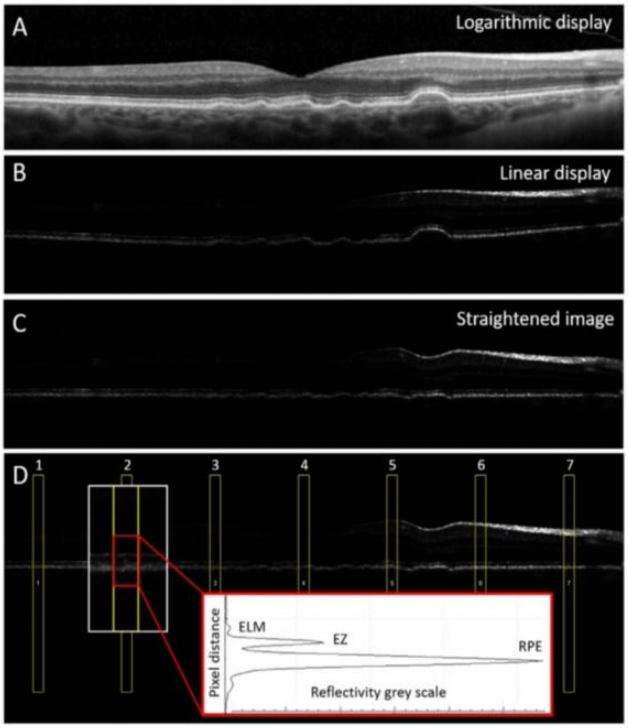

Figure 3: Example of a SD-OCT horizontal line scan. Reprinted from (Thiele et al., 2020), Transl Vis Sci Technol, 9(11):17. https://doi.org/10.1167/tvst.9.11.17. Licensed under CC BY-NC-ND 4.0. (A) line scan in logarithmic display. (B) line scan in linear display (raw image date). (C) The SD-OCT image was straightened according to segmentation coordinates of the RPE. (D) The rEZR was determined on the straightened SD-OCT raw images by assessing the peak value of the EZ and the ELM in corresponding reflectivity profile. A magnified ROI is shown in the rectangular box. Please note: The primary outcome of our study is the mean rEZR, obtained at adjoining ROIs, which is calculated for the entire scan volume as well as for the hemispheric regions. This figure is provided to illustrate how the ROIs were defined and obtained in our study.

In each B-scan, rEZR values were calculated based on pixel reflectance, quantified as pixel intensity (dynamic range of gray values: 0–1 [arbitrary units (Unterlauft et al.,)]), within the adjoining region of interest (ROI). Unlike our approach, where ROIs were defined continuously, our co-reseracher (ST) employed non-continuous ROIs for her analysis (Thiele et al., 2020) (Figure 3D). Each of our ROIs was defined with a width of 20 pixels, corresponding to approximately 120 µm in high-speed SD-OCT imaging. To assess rEZR in the global scan region and inter-hemisphere region, the scan volume was divided into superior and inferior hemispheres using the fovea-disc axis as the reference.

This segmentation facilitated subsequent comparisons of rEZR between the hemispheres. It is important to emphasize that during inter-hemisphere comparisons, defects in the superior hemisphere correspond to the analysis of rEZR, RNFL, and GCL in the inferior region of near-infrared reflectance imaging. Similarly, defects in the inferior hemisphere correspond to the analysis of rEZR, RNFL, and GCL in the superior region of near-infrared reflectance imaging (Figure 4). This relationship is determined by the characteristic of glaucomatous visula field damage, where structural changes in the inferior retina correspond to functional deficits in the superior VF.

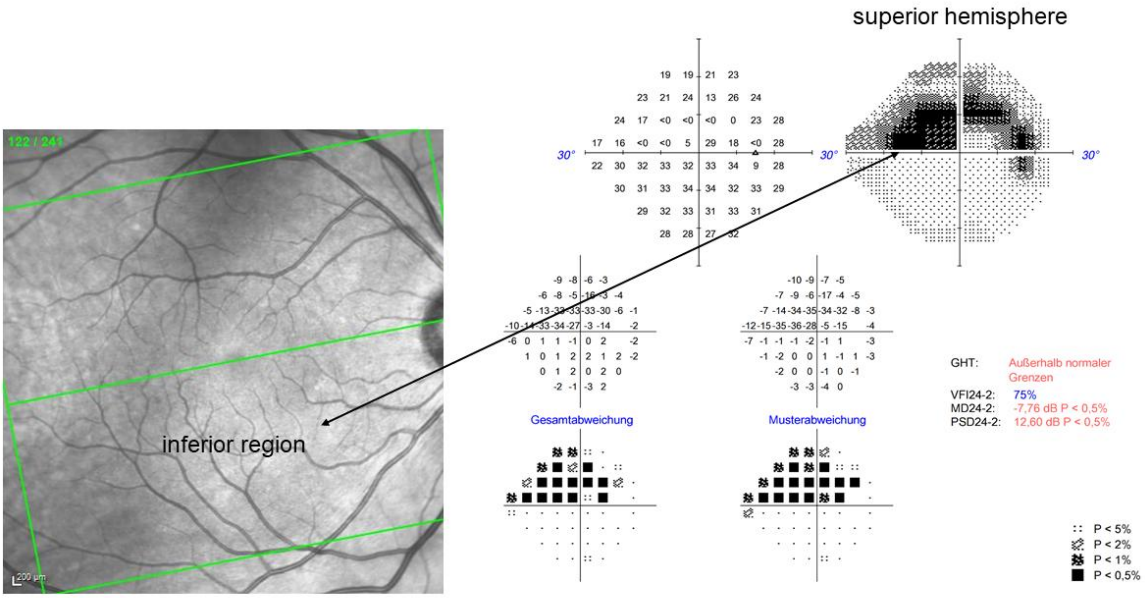

Figure 4: Illustration of Structural and Functional Deficits in glaucoma: VF defects in the superior hemisphere correspond to structural retinal damage in the inferior region.

2.4 Analysis of RNFL and GCL

Prior to conducting the inter-hemisphere comparison of rEZR, an inter-hemisphere analysis of RNFL and GCL was performed. Based on the characteristics of VF defects (Figure 1), the hemisphere exhibiting VF damage was defined as the affected

hemisphere, while the opposing side was designated as the unaffected hemisphere. The differences in RNFL and GCL thickness between the affected and unaffected hemispheres were then analyzed and compared.

2.5 Statistical Analysis

The statistical analyses in this study followed a structured, multilevel approach to evaluate the relationship between rEZR values and glaucoma-related retinal changes. First, descriptive statistics were used to summarize demographic characteristics (e.g., age, gender) and baseline measurements stratified by diagnostic group (control, NTG, POAG). Linear regression and linear mixed-effects models were then performed to compare global and hemispheric rEZR values between groups (case vs. control, NTG vs. POAG), adjusting for relevant covariates such as age, gender, mean GCL thickness, and RNFL measurements. Within-patient comparisons between affected and unaffected hemispheres were also performed using mixed models, taking into account the hierarchical structure of the data (hemispheres within individuals).

Regression analysis started with univariable models and stepwise added covariates to multivariable models, including gender, age, and educational characteristics as these variables are known to influence retinal thickness and may differ between diagnostic groups. Model performance was assessed using marginal and conditional R^2 values, and the interpretation of model coefficients focused on estimated differences in mean rEZR between hemispheres and diagnostic groups. Subgroup analyses also examined early vs. advanced damage and specific patterns of hemispheric involvement.

Mixed-effects models were estimated to adequately address the non-independence of observations resulting from bilateral retinal measurements within the same individuals. This approach allows the estimation of fixed effects (e.g., diagnostic group, hemisphere)

and random effects that capture patient-specific variability. By including random intercepts for patient ID, the model accounts for intra-subject correlation arising from repeated measurements within individuals.

In a further analysis step, mean GCL and RNFL values were included to account for structural differences in retinal anatomy that may influence rEZR. This adjustment helps to distinguish whether observed differences in rEZR are due to the disease status itself or to changes in retinal morphology. Model performance was assessed using marginal and conditional R^2 values to distinguish between the variance explained by fixed effects alone and the total variance explained by random effects. This assessment ensured that the model extensions made a meaningful contribution to the explanatory power.

All statistical analyses were performed using R 4.1 (R Core Team, 2020). Linear regression and mixed-effects models were implemented using the lm() function from base R and the lmer() function from the lme4 package (Bates et al., 2015). Model performance was assessed using marginal and conditional R^2 values calculated with the MuMIn package (Bartoń, 2025) and the r.squaredGLMM() function. P-values were based on two-sided tests, with significance set at $p < 0.05$. For mixed models, p-values were approximated using the lmerTest package (Kuznetsova et al., 2017).

3. Results

Eighty-six eyes of 86 subjects were recruited in this study, including 21 NTG eyes, 39 POAG eyes and 26 normal eyes. Table 1A presents the distribution of participants with glaucoma in our study. Patients with POAG and NTG were classified into three groups based on disease severity: a significantly affected group, an early glaucoma group, and a preperimetric group (early-stage glaucoma without detectable VF defects). The significantly affected group was further categorized into isolated superior, isolated inferior, and both hemispheres based on the hemisphere affected in the VF. Similarly, the early glaucoma group was subcategorized into isolated superior, isolated inferior, both hemispheres, and paracentral involvement according to the affected hemisphere identified in the VF. Among participants in the significantly affected group, 13 had isolated superior defects (6 POAG and 7 NTG), 10 had isolated inferior defects (8 POAG and 2 NTG), while 8 had defects in both hemispheres (all POAG). In the early glaucoma group, 7 participants had isolated superior defects (3 POAG and 4 NTG), 5 had isolated inferior defects (2 POAG and 3 NTG), 7 had defects in both hemispheres (5 POAG and 2 NTG) and 3 had paracentral involvement (1 POAG and 2 NTG). Pre-perimetric glaucoma cases included 6 POAG and 1 NTG, totaling 7 participants.

Table 1: Distribution of glaucoma subgroups by affected hemisphere across different comparison groups. (A) shows the classification of all glaucoma patients in this study (n = 60; POAG: 39, NTG: 21) based on glaucoma subtype, VF defect severity, and defect pattern (isolated sup. , isolated inf. , both and paracentral). Patients are categorized into significantly affected group, early glaucoma group and pre-perimetric group. Glaucoma cases with VF defects - excluding pre-perimetric and paracentral groups - totaled 50 cases (32 POAG, 18 NTG), including 31 cases (22 POAG, 9 NTG) in the significantly affected group. (B) shows glaucoma cases with isolated hemisphere involvement (superior or inferior) within both the significantly affected group and early glaucoma group.

A	significantly affected group			early glaucoma group				pre-perimetric group
Affected hemisphere	Isolated sup.	Isolated inf.	both	Isolated sup.	Isolated inf.	both	parace-ntral	
POAG	6	8	8	3	2	5	1	6
NTG	7	2	0	4	3	2	2	1
Total	13	10	8	7	5	7	3	7

B	significantly affected group		early glaucoma group	
Affected hemisphere	Isolated sup.	Isolated inf.	Isolated sup.	Isolated inf.
glaucoma cases	13	10	7	5

3.1 Comparison of the rEZR between control group and glaucoma cases

In this grouping analysis, we not only compared the rEZR between the control group and all glaucoma cases but also conducted separate comparisons of the rEZR between the control group and POAG, as well as NTG cases.

3.1.1 Relationship of rEZR between controls and glaucoma cases

There was no statistically significant difference in mean rEZR between control subjects and glaucoma cases (n = 60). However, the box plots (Figure 5A) suggested a trend toward lower median rEZR values in glaucoma cases (~ 45) compared to controls (~ 55),

with NTG and POAG subgroups (panel A, right) showing similar downward trends. To further investigate this, multiple linear regression analyses were conducted through three sequential models: a univariable model (Model 1), a model adjusted for age and sex (Model 2), and a fully adjusted model that also included mean GCL and RNFL thickness (Model 3).

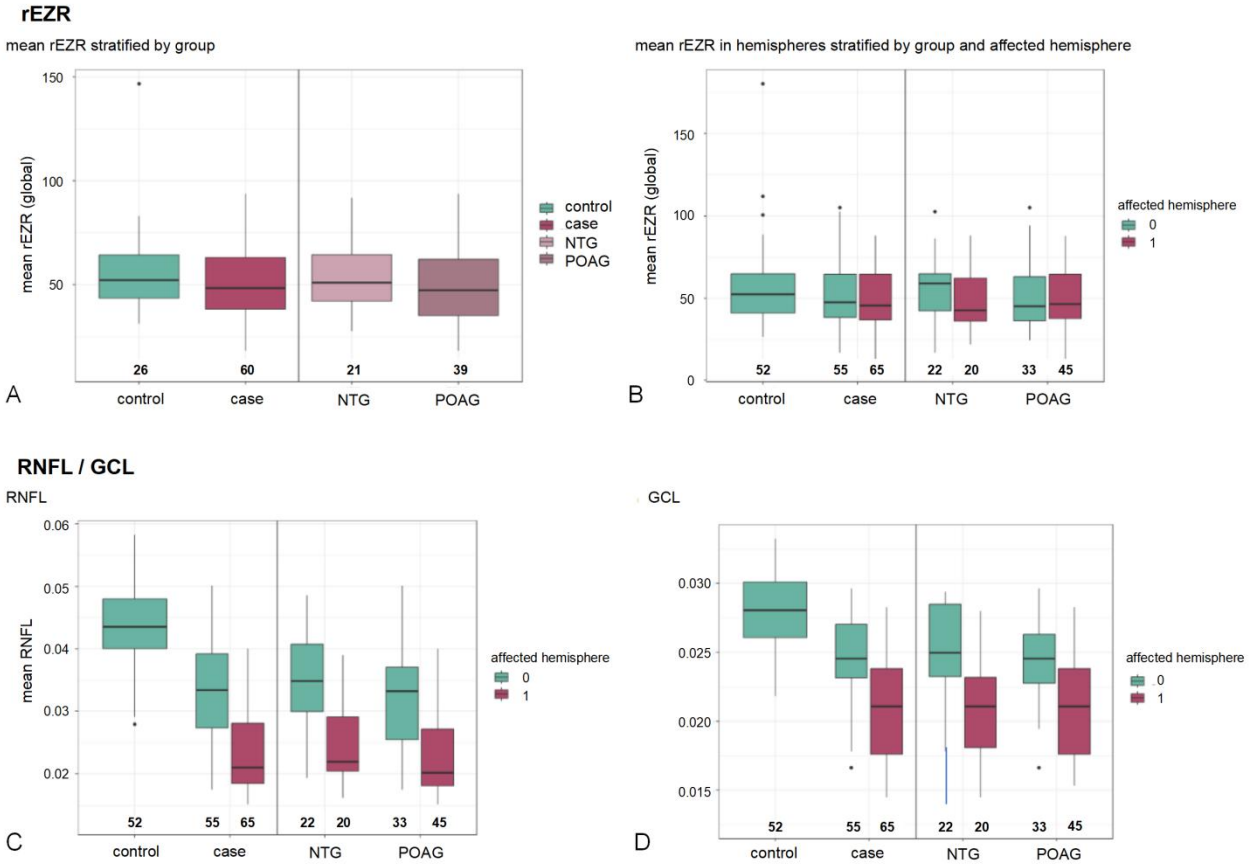

Figure 5: Box plots comparing mean rEZR, RNFL, and GCL between diagnostic groups and hemispheres. (A) Mean rEZR stratified by diagnostic group (control, glaucoma, NTG, POAG). (B) Mean rEZR in hemispheres stratified by group and affected hemisphere (0 = unaffected, 1 = affected). (C) Mean RNFL thickness in each hemisphere across groups. (D) Mean GCL thickness in each hemisphere across groups. Box plots indicate the median, interquartile range, and outliers. Numbers below each group indicate sample sizes. Color represents both diagnostic group and hemisphere status (affected vs. unaffected). A reduction in rEZR, RNFL, and GCL is observed in glaucoma groups and affected hemispheres.

In Model 1, glaucoma cases showed a non-significant trend toward reduced rEZR

compared with controls (Estimate = -9.35; 95 % CI: -19.58 to -0.88; p = 0.072). After adjusting for age and sex in Model 2, the association persisted as borderline significant (Estimate = -9.02; 95 % CI: -18.70 to -0.66; p = 0.067). However, in Model 3, after further adjusting for mean GCL and RNFL thickness, the association became clearly non-significant (p = 0.541). This suggests that differences in GCL and RNFL thickness may explain the initially observed trend between groups. Notably, age remained a significant predictor of reduced rEZR in the fully adjusted model (p = 0.017) (Table 2A).

The forest plot (Figure 6A) visually reinforces these findings, demonstrating that the confidence intervals (CI) for mean GCL and RNFL thickness cross zero, indicating their non-significant contributions after full adjustment.

Table 2: Multivariate linear regression models assessing mean rEZR in glaucoma cases and subtypes (NTG and POAG). Results of three sequential linear regression models evaluating predictors of rEZR. (A) Comparison between controls and glaucoma cases. (B) Comparison between controls and glaucoma subtypes: NTG and POAG. Model 1: univariable analysis, Model 2: adjusted for age and sex, Model 3: further adjusted for mean GCL and RNFL thickness. Estimates are presented with 95 % CI. Statistically significant predictors ($p < 0.05$) are indicated in bold. Age consistently shows a significant negative association with rEZR, while glaucoma status and subtypes do not show significant differences after full adjustment. Note: Global mean GCL and RNFL thickness values were included as predictors in the case-control regression A, while hemisphere mean GCL and RNFL predictors were used in the subtype comparison B to account for possible regional variation in structural damage.

A

	Model 1: univariable			**Model 2: age & sex adjusted**			**Model 3: + GCL & RNFL adjusted**		
Predictors	*Estimates*	*CI*	*p*	*Estimates*	*CI*	p	Estimates	CI	p
(Intercept)	57.01	49.47 – 64.56	**<0.001**	110.02	70.04 – 150.00	**<0.001**	108.66	67.60 – 149.72	**<0.001**
cc [case]	-9.35	-19.58 – 0.88	0.072	-9.02	-18.70 – 0.66	0.067	-5.97	-25.43 – 13.49	0.541
age				-0.78	-1.42 – -0.14	**0.018**	-0.79	-1.44 – -0.15	**0.017**
gender [M]				-8.60	-18.97 – 1.77	0.102	-8.21	-18.98 – 2.57	0.132
mean GCL global							7.94	-5.52 – 21.39	0.242
mean RNFL global							-5.47	-21.97 – 11.03	0.509
Observations	57			57			57		
R^2 / R^2 adjusted	0.058 / 0.040			0.189 / 0.143			0.214 / 0.137		

B

	Model 1: univariable			**Model 2: age & sex adjusted**			**Model 3: + GCL & RNFL adjusted**		
Predictors	*Estimates*	*CI*	*p*	*Estimates*	*CI*	p	Estimates	CI	p
(Intercept)	57.01	49.40 – 64.63	**<0.001**	110.84	70.41 – 151.26	**<0.001**	113.89	71.80 – 155.97	**<0.001**
group [NTG]	-9.35	-24.37 – 5.67	0.217	-11.62	-26.04 – 2.81	0.112	-7.89	-31.06 – 15.28	0.497
group [POAG]	-9.35	-20.60 – 1.90	0.101	-7.97	-18.64 – 2.69	0.140	-4.96	-25.59 – 15.66	0.631
age				-0.79	-1.43 – -0.14	**0.018**	-0.87	-1.53 – -0.22	**0.010**
gender [M]				-9.22	-19.98 – 1.53	0.091	-8.72	-19.77 – 2.33	0.119
mean GCL hemisphere							9.70	-3.15 – 22.56	0.136
mean RNFL hemisphere							-7.12	-22.77 – 8.53	0.365
Observations	57			57			57		
R^2 / R^2 adjusted	0.058 / 0.023			0.193 / 0.131			0.230 / 0.138		

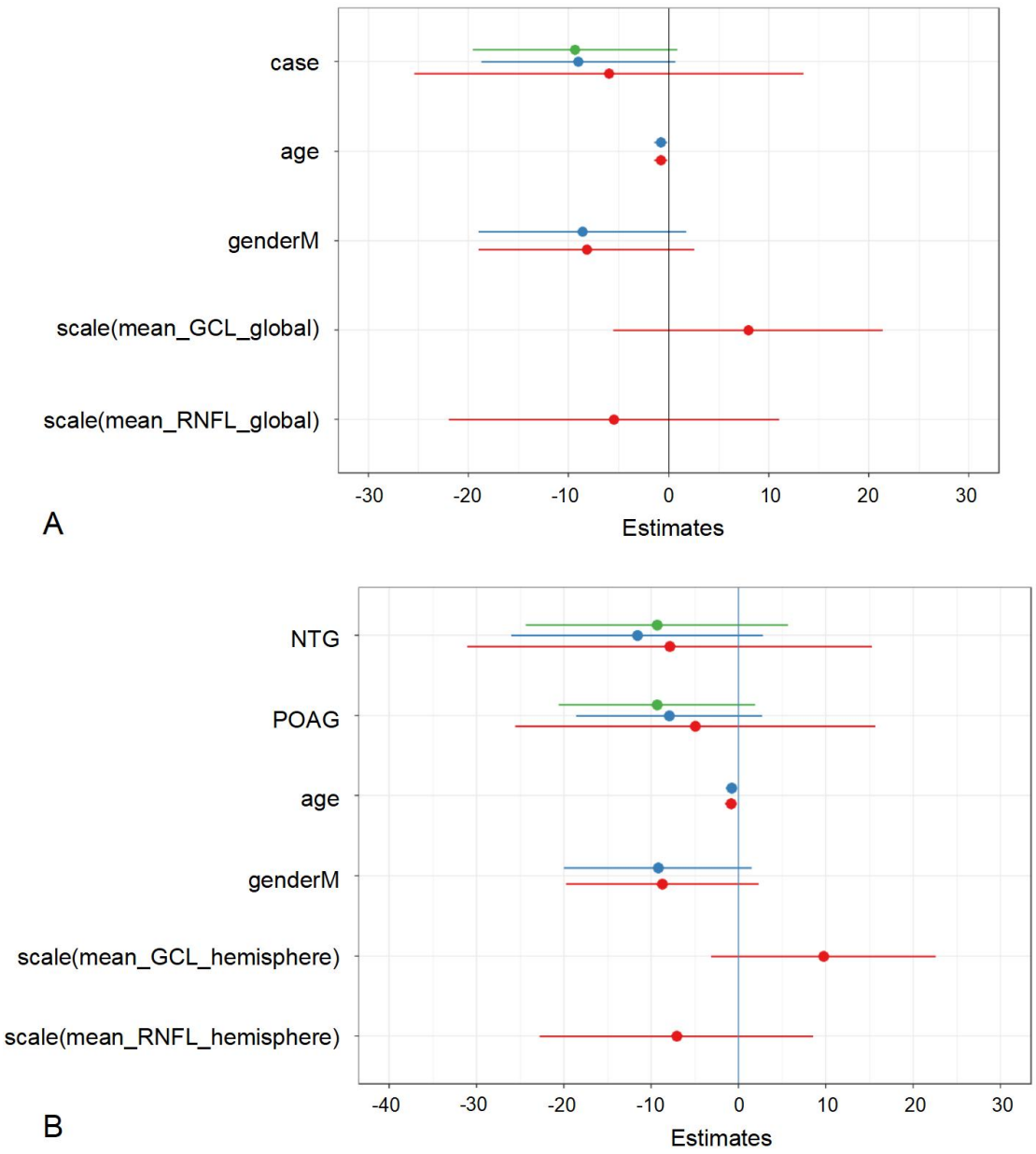

Figure 6: Forest plots illustrating regression estimates for rEZR across controls and glaucoma subtypes, corresponding to Table 2A-B. (A) Comparison between controls and glaucoma cases. (B) Comparison between controls and glaucoma subtypes: NTG and POAG. Each point represents the estimated regression coefficient (Estimate) for a given predictor, with horizontal lines indicating the 95 % CI. Green indicates univariable models (Model 1), blue indicates models adjusted for age and sex (Model 2), and red represents further adjusted for mean GCL and RNFL thickness (Model 3). CIs that cross zero indicate no statistically significant association. These visualizations confirm that neither glaucoma group nor subtype showed significant differences in rEZR compared to controls after full adjustment, while age remained a consistent negative predictor.

3.1.2 Relationship of rEZR between controls and glaucoma subtypes

Further subgroup analysis revealed no meaningful difference in rEZR between the control group and either of the glaucoma subtypes - NTG and POAG. As shown in Table 2B, both subgroups exhibited non-significant trends toward reduced rEZR in the unadjusted model (Model 1), with p-values of 0.217 for NTG and 0.101 for POAG. These associations remained statistically insignificant even after adjusting for age and sex in Model 2 (NTG: $p = 0.112$; POAG: $p = 0.140$).

Of note, age continued to be a consistent and significant factor associated with lower rEZR levels in both adjusted models (Model 2: $p = 0.018$; Model 3: $p = 0.010$). The corresponding forest plot (Figure 6B) aligns with these statistical results, showing that the CI for both NTG and POAG intersect the null value, reinforcing the lack of a significant group effect. While a downward trend in rEZR was observable among glaucoma patients, no distinct separation was evident between the two subtypes.

3.2 Comparison of the rEZR between control group and glaucoma cases with visual field defects

To assess whether rEZR is altered in retinal regions with pronounced functional impairment, we compared rEZR values between the control group and glaucoma patients exhibiting VF defects. In this analysis, glaucoma cases with VF defects were divided into two subgroups: the significantly affected group and the early glaucoma group. We first compared rEZR between the control group and all glaucoma patients with VF defects. Subsequently, a separate comparison was performed between the control group and only those in the significantly affected group.

3.2.1 In glaucoma cases with visual field defects

A total of 50 glaucoma patients with VF defects were included in this analysis, comprising 32 individuals with POAG and 18 with NTG (Table 1A). We first compared the rEZR between the control group and the combined group of glaucoma patients. Additionally, separate comparisons were conducted between the control group and each glaucoma subtype (POAG and NTG) individually.

3.2.1.1 Relationship of rEZR between control group and glaucoma cases with visual field defects

There was no statistically significant difference in rEZR between the control group and glaucoma cases with VF defects (n = 50). In the univariable model (Model 1), the glaucoma group (cc) showed a trend toward reduced rEZR, though this did not reach statistical significance (Estimate = -8.13, p = 0.097). After adjusting for age and gender in Model 2, the estimated effect remained comparable (p = 0.078), while age emerged as a significant negative predictor of rEZR (Estimate = -0.67, 95 % CI: -1.24 to -0.09, p = 0.023). (Table 3A).

In the fully adjusted model (Model 3), the association between glaucoma status and rEZR remained non-significant (Estimate = -7.24, p = 0.341). However, age continued to show a significant negative association with rEZR (Estimate = -0.64, p = 0.028), while both GCL and RNFL thickness were not statistically significant predictors.

These findings are visually supported by the forest plot (Figure 7A), where the CI for the glaucoma group includes zero, confirming the lack of statistical significance. Together, these results suggest that although glaucoma patients with VF defects tend to have lower rEZR values than controls, this difference is not statistically significant after adjusting for relevant covariates. Age remains the most consistent and significant predictor of reduced rEZR.

Table 3: Multivariate linear regression models assessing mean rEZR in glaucoma cases with VF defects. (A) Controls vs. all glaucoma cases with VF defects. (B) Controls vs. NTG and POAG with VF defects. Regression coefficients (Estimates), 95 % CI, and p-values are reported for three models: univariable (Model 1), adjusted for age and sex (Model 2), and further adjusted for mean GCL and RNFL thickness (Model 3). Statistically significant p-values ($p < 0.05$) are shown in bold.

A

	Model 1: univariable			Model 2: age & sex adjusted			Model 3: + GCL & RNFL adjusted		
Predictors	*Estimates*	*CI*	*p*	*Estimates*	*CI*	p	Estimates	CI	p
(Intercept)	56.95	49.31 – 64.58	**<0.001**	102.60	66.60 – 138.60	**<0.001**	100.62	63.60 – 137.63	**<0.001**
cc [case]	-8.13	-17.76 – 1.49	0.097	-8.33	-17.60 – 0.95	0.078	-7.24	-22.25 – 7.76	0.341
age				-0.67	-1.24 – -0.09	**0.023**	-0.64	-1.22 – -0.07	**0.028**
gender [M]				-8.11	-17.55 – 1.33	0.091	-8.00	-17.60 – 1.61	0.102
mean GCL hemisphere							4.28	-4.29 – 12.86	0.324
mean RNFL hemisphere							-3.04	-13.41 – 7.32	0.562
Random Effects									
σ^2	154.31			153.95			156.35		
τ_{00}	309.07 $_{PID}$			278.84 $_{PID}$			279.00 $_{PID}$		
ICC	0.67			0.64			0.64		
N	76 $_{PID}$			76 $_{PID}$			76 $_{PID}$		
Observations	117			117			117		
Marginal R^2 / Conditional R^2	0.034 / 0.678			0.112 / 0.684			0.118 / 0.683		

B

	Model 1: univariable			Model 2: age & sex adjusted			Model 3: + GCL & RNFL adjusted		
Predictors	*Estimates*	*CI*	*p*	*Estimates*	*CI*	p	Estimates	CI	p
(Intercept)	56.95	49.26 – 64.63	**<0.001**	102.71	66.48 – 138.95	**<0.001**	100.72	63.46 – 137.98	**<0.001**
group [NTG]	-7.79	-20.40 – 4.83	0.224	-9.07	-21.37 – 3.22	0.147	-7.85	-24.82 – 9.12	0.361
group [POAG]	-8.32	-18.92 – 2.27	0.122	-7.95	-18.14 – 2.25	0.125	-6.96	-22.66 – 8.75	0.382
age				-0.67	-1.24 – -0.09	**0.024**	-0.64	-1.22 – -0.07	**0.029**
gender [M]				-8.25	-17.88 – 1.38	0.092	-8.11	-17.89 – 1.68	0.104
mean GCL hemisphere							4.26	-4.36 – 12.87	0.330
mean RNFL hemisphere							-3.03	-13.44 – 7.39	0.566
Random Effects									
σ^2	154.62			154.34			156.75		
τ_{00}	314.05 $_{PID}$			283.27 $_{PID}$			283.60 $_{PID}$		
ICC	0.67			0.65			0.64		
N	76 $_{PID}$			76 $_{PID}$			76 $_{PID}$		
Observations	117			117			117		
Marginal R^2 / Conditional R^2	0.034 / 0.681			0.111 / 0.686			0.117 / 0.686		

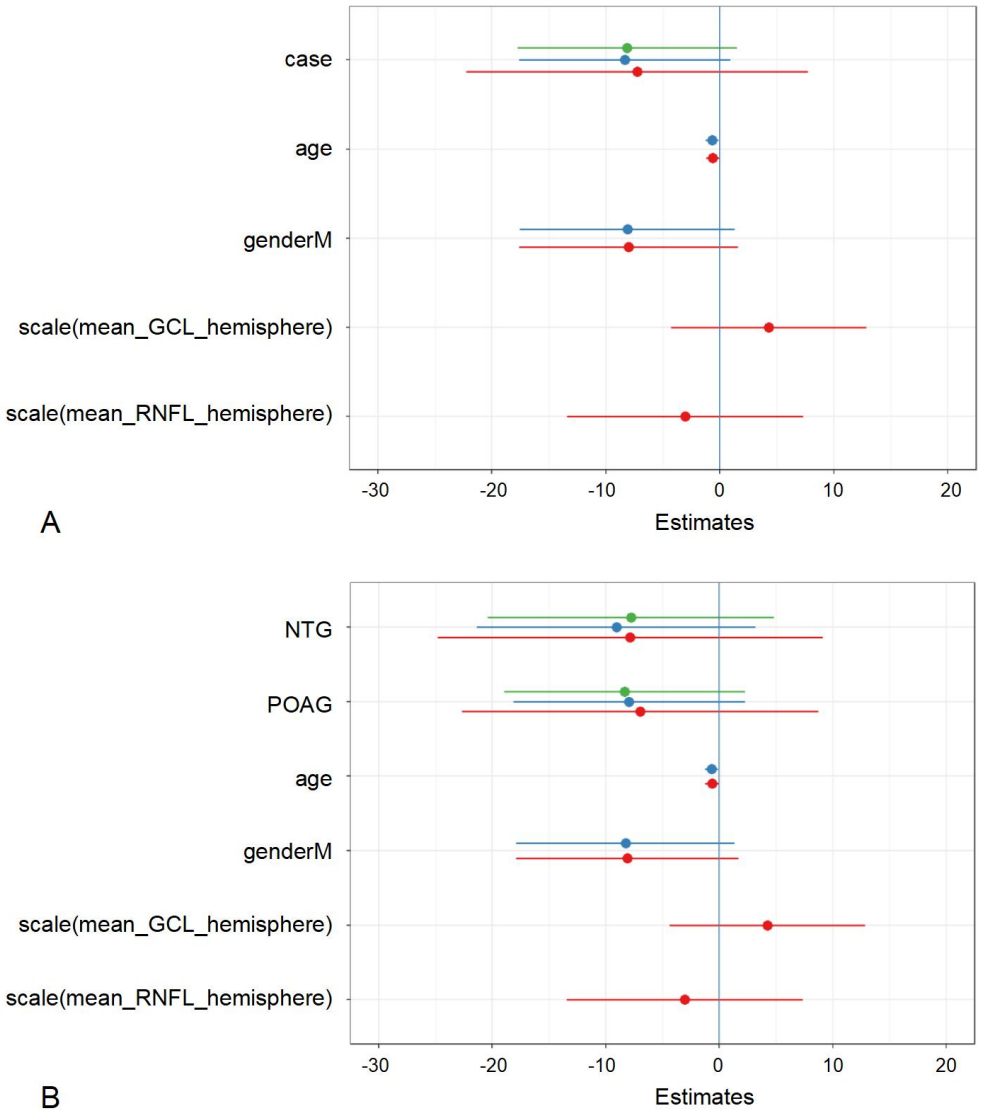

Figure 7: Forest plots illustrating regression estimates for rEZR across controls and glaucoma cases with VF defects, corresponding to Table 3A-B. (A) Controls vs. all glaucoma cases with VF defects. (B) Controls vs. NTG and POAG (within VF defect group). Estimates and 95 % CIs are shown for each group across three models. Full model details and variable definitions are provided in the legend of Figure 6.

3.2.1.2 Relationship of rEZR between control group and subtypes glaucoma

When stratified by glaucoma subtype, no statistically significant differences in rEZR were found between the control group and either the NTG (n = 18) or POAG (n = 32) groups. Both subtypes showed a trend toward lower rEZR values compared to controls in the

univariable analysis, but these differences did not reach statistical significance.

After adjusting for age, sex, and retinal structural measures (GCL and RNFL thickness), the associations for both NTG and POAG remained non-significant across all models (Table 3B). The forest plot (Figure 7B) further supports these findings, as the CIs for both subtypes cross zero, indicating no meaningful distinction in rEZR compared to the control group.

These results suggest that while rEZR values tend to be lower in glaucoma subtypes, the differences are not statistically meaningful after adjusting for age, sex, and structural retinal measures.

3.2.2 In significantly affected group

This subgroup included 31 glaucoma patients with pronounced VF defects (22 POAG and 9 NTG; Table 1A). We evaluated differences in rEZR between the control group and this subset of glaucoma patients and further assessed rEZR separately in POAG and NTG cases within the significantly affected group.

3.2.2.1 Relationship of rEZR between control group and significantly affected group

In glaucoma patients with severe VF impairment (n = 31), rEZR appeared lower than in controls; however, this difference did not reach statistical significance in any of the regression models. Although the unadjusted analysis suggested a borderline association ($p = 0.064$) (Table 4A), adjustment for age and gender produced minimal change in effect size, and the result remained non-significant. Further inclusion of GCL and RNFL hemispheric thickness in the model attenuated the group difference even more ($p = 0.315$).

Table 4: Multivariate linear regression models assessing mean rEZR in significantly affected glaucoma group. (A) Controls vs. significantly affected glaucoma group. (B) Controls vs. NTG and POAG in significantly affected group. Regression coefficients (Estimates), 95 % CI, and p-values are reported for three models: univariable (Model 1), adjusted for age and sex (Model 2), and further adjusted for mean GCL and RNFL thickness (Model 3). Statistically significant p-values ($p < 0.05$) are shown in bold.

A

	Model 1: univariable			Model 2: age & sex adjusted			Model 3: + GCL & RNFL adjusted		
Predictors	*Estimates*	*CI*	*p*	*Estimates*	*CI*	p	Estimates	CI	p
(Intercept)	56.95	49.11 – 64.78	**<0.001**	118.35	74.09 – 162.61	**<0.001**	120.17	74.64 – 165.71	**<0.001**
cc [case]	-10.39	-21.38 – 0.60	0.064	-9.99	-20.48 – 0.49	0.061	-11.72	-34.79 – 11.36	0.315
age				-0.96	-1.67 – -0.25	**0.009**	-0.98	-1.69 – -0.26	**0.008**
gender [M]				-5.42	-16.71 – 5.88	0.343	-5.36	-17.01 – 6.29	0.363
mean GCL hemisphere							4.77	-6.26 – 15.81	0.392
mean RNFL hemisphere							-5.41	-18.59 – 7.76	0.416
Random Effects									
σ^2	174.28			171.62			173.76		
τ_{00}	317.09 $_{PID}$			279.56 $_{PID}$			283.24 $_{PID}$		
ICC	0.65			0.62			0.62		
N	57 $_{PID}$			57 $_{PID}$			57 $_{PID}$		
Observations	91			91			91		
Marginal R^2 / Conditional R^2	0.052 / 0.664			0.146 / 0.675			0.150 / 0.677		

B

	Model 1: univariable			Model 2: age & sex adjusted			Model 3: + GCL & RNFL adjusted		
Predictors	*Estimates*	*CI*	*p*	*Estimates*	*CI*	p	Estimates	CI	p
(Intercept)	56.95	49.05 – 64.84	**<0.001**	119.33	74.76 – 163.90	**<0.001**	121.20	75.36 – 167.04	**<0.001**
group [NTG]	-12.42	-29.18 – 4.34	0.144	-13.94	-30.20 – 2.32	0.092	-15.78	-42.04 – 10.49	0.236
group [POAG]	-9.62	-21.68 – 2.43	0.116	-8.51	-20.03 – 3.00	0.145	-10.21	-33.87 – 13.45	0.393
age				-0.96	-1.68 – -0.25	**0.009**	-0.98	-1.70 – -0.26	**0.008**
gender [M]				-6.24	-17.89 – 5.40	0.289	-6.21	-18.19 – 5.78	0.306
mean GCL hemisphere							4.83	-6.25 – 15.91	0.389
mean RNFL hemisphere							-5.47	-18.69 – 7.75	0.413
Random Effects									
σ^2	174.99			172.27			174.43		
τ_{00}	322.71 $_{PID}$			282.65 $_{PID}$			286.33 $_{PID}$		
ICC	0.65			0.62			0.62		
N	57 $_{PID}$			57 $_{PID}$			57 $_{PID}$		
Observations	91			91			91		
Marginal R^2 / Conditional R^2	0.051 / 0.666			0.148 / 0.677			0.152 / 0.679		

Throughout the models, age consistently showed a statistically significant association with lower rEZR values. The forest plot (Figure 8A) illustrates these findings, with CIs for glaucoma status overlapping zero in all cases. Overall, while a reduction in rEZR was observed among patients with more advanced functional loss, this was not statistically supported after accounting for demographic and structural factors.

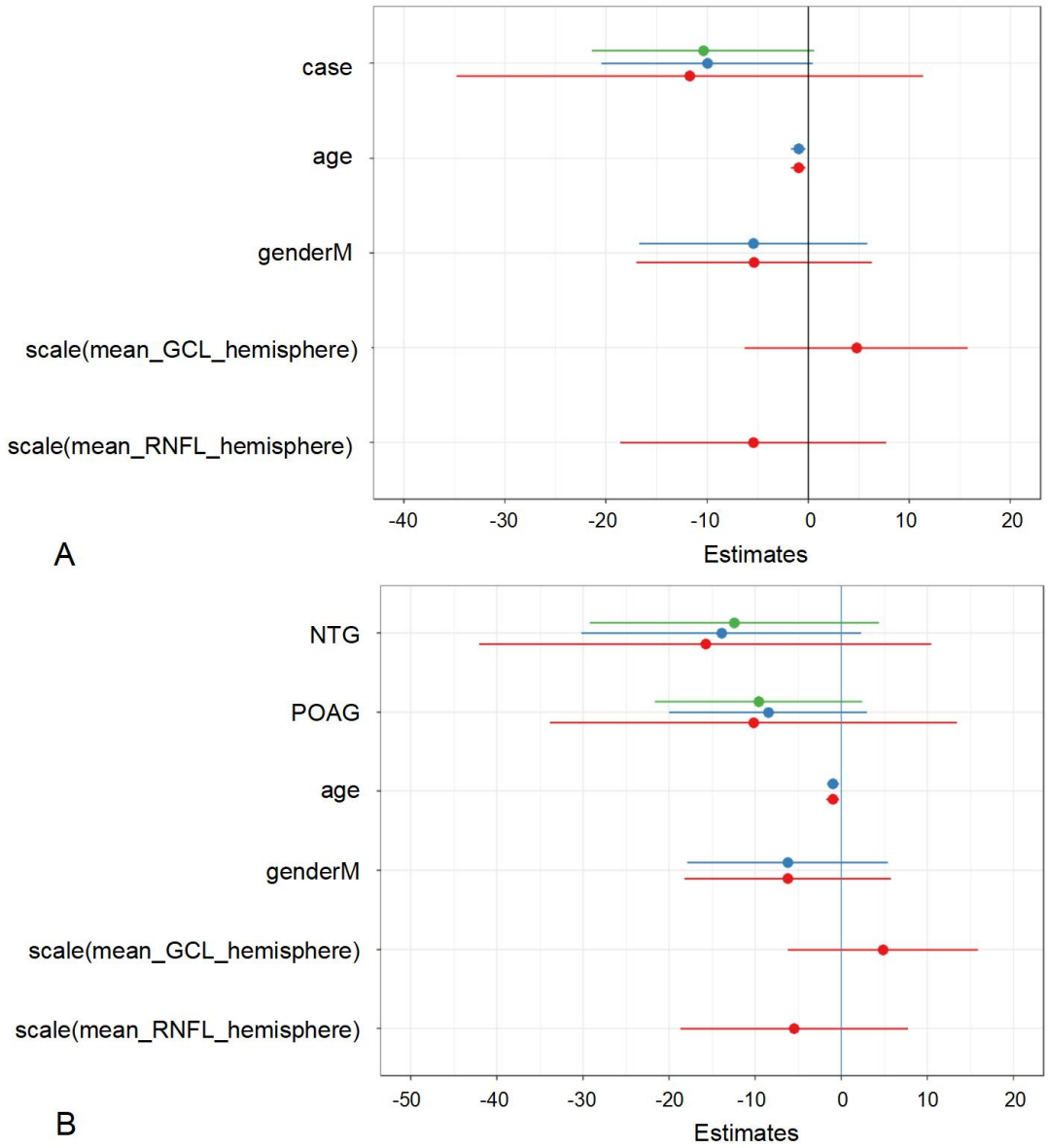

Figure 8: Forest plots illustrating regression estimates for rEZR across controls and significantly affected glaucoma group, corresponding to Table 4A-B. (A) Controls vs. significantly affected glaucoma group. (B) Controls vs. NTG and POAG (within significantly affected group). Estimates and 95 % CIs are shown for each group across three models. Full model details and variable definitions are provided in the legend of Figure 6.

3.2.2.2 Relationship of rEZR between control group and subtypes glaucoma

Within the significantly affected group, neither NTG (n = 9) nor POAG (n = 22) cases showed a statistically significant difference in rEZR compared to controls (Table 4B).

Across all regression models, both subtypes exhibited a consistent trend toward lower rEZR values, but the associations did not reach significance.

Adjustments for age, gender, and hemispheric GCL and RNFL thickness did not materially change the results. Although age continued to show an inverse correlation with rEZR, this pattern had already been observed in earlier analyses. As illustrated in the forest plot (Figure 8B), the CIs for both NTG and POAG groups crossed zero, further supporting the absence of meaningful group-level differences. Measures of GCL and RNFL thickness were also not associated with rEZR in this subgroup.

Overall, while the data suggest a directional reduction in rEZR among glaucoma subtypes with pronounced VF loss, these effects were not statistically supported after accounting for structural and demographic variables.

3.3 Comparison of RNFL and GCL between affected and unaffected hemispheres

To better understand the relationship between structural and functional changes in glaucoma, affected hemispheres were categorized based on VF defects into three groups: isolated superior, isolated inferior, and both hemispheres involved. RNFL and GCL thickness were then compared between the affected and unaffected hemispheres across all participants (57 glaucoma patients and 26 controls), excluding three glaucoma cases with paracentral defects.

3.3.1 Relationship of RNFL and GCL between affected and unaffected hemispheres

Across all individuals excluding those with paracentral VF defects, significant inter-hemispheric differences were observed in both RNFL and GCL thickness. As shown in Figure 5C and 5D, RNFL and GCL values were consistently reduced in the affected

hemisphere among glaucoma patients - including both NTG and POAG - while controls exhibited no hemispheric difference.

For RNFL (Table 5A), the affected hemisphere showed a robust reduction in thickness across all models. The association remained statistically significant after adjusting for age and gender (Model 2), as well as after further accounting for GCL thickness in Model 3 ($p < 0.001$). Notably, GCL thickness emerged as a strong independent predictor of RNFL in the fully adjusted model ($p < 0.001$), suggesting structural interdependence between layers.

In contrast, while GCL thickness was also significantly lower in the affected hemisphere in unadjusted and age-sex adjusted models (Table 5B), this relationship was no longer significant after controlling for RNFL thickness (Model 3: $p = 0.921$). This attenuation suggests that GCL thinning may reflect upstream changes in RNFL or shared structural variation, rather than an independent hemispheric effect.

These patterns are further visualized in the forest plots (Figure 9A and 9B). Affected hemisphere status remains a consistent predictor of RNFL reduction across all models, while the corresponding effect on GCL disappears in the fully adjusted analysis. Together, these findings indicate that RNFL thickness is more consistently and independently associated with hemispheric differences, while GCL changes may be mediated through RNFL or other covariates.

Table 5: Multivariate linear regression models assessing RNFL and GCL thickness differences between affected and unaffected hemispheres. (A) RNFL thickness as the dependent variable. (B) GCL thickness as the dependent variable. Regression coefficients (Estimates), 95 % CI, and p-values are reported for three models: Model 1 (univariable), Model 2 (adjusted for age and sex), and Model 3 (further adjusted for the other retinal layer: GCL in A, RNFL in B). Statistically significant p-values ($p < 0.05$) are indicated in bold.

A

RNFL

	Model 1: univariable			Model 2: age & sex adjusted			Model 3: + GCL & RNFL adjusted		
Predictors	*Estimates*	*CI*	*p*	*Estimates*	*CI*	p	Estimates	CI	p
(Intercept)	0.16	-0.02 – 0.35	0.087	0.22	-1.23 – 1.67	0.766	-0.09	-0.72 – 0.54	0.781
affected hem	-0.81	-1.00 – -0.62	**<0.001**	-0.81	-1.00 – -0.61	**<0.001**	-0.28	-0.43 – -0.12	**<0.001**
age				0.00	-0.02 – 0.02	0.973	0.00	-0.01 – 0.01	0.509
gender [M]				-0.12	-0.51 – 0.27	0.543	-0.09	-0.26 – 0.08	0.277
mean GCL hemisphere							0.83	0.75 – 0.92	**<0.001**
Random Effects									
σ^2	0.18			0.18			0.11		
τ_{00}	0.66 $_{PID}$			0.67 $_{PID}$			0.09 $_{PID}$		
ICC	0.78			0.79			0.46		
N	86 $_{PID}$			86 $_{PID}$			86 $_{PID}$		
Observations	172			172			172		
Marginal R^2 / Conditional R^2	0.113 / 0.807			0.115 / 0.811			0.795 / 0.890		

B

GCL

	Model 1: univariable			Model 2: age & sex adjusted			Model 3: + GCL & RNFL adjusted		
Predictors	*Estimates*	*CI*	*p*	*Estimates*	*CI*	p	Estimates	CI	p
(Intercept)	0.13	-0.06 – 0.33	0.179	0.37	-1.15 – 1.90	0.631	0.19	-0.49 – 0.87	0.584
affected hem	-0.66	-0.83 – -0.48	**<0.001**	-0.66	-0.83 – -0.48	**<0.001**	0.01	-0.15 – 0.16	0.921
age				-0.00	-0.03 – 0.02	0.773	-0.00	-0.01 – 0.01	0.483
gender [M]				-0.03	-0.44 – 0.38	0.880	0.07	-0.11 – 0.25	0.455
mean RNFL hemisphere							0.84	0.75 – 0.92	**<0.001**
Random Effects									
σ^2	0.15			0.15			0.10		
τ_{00}	0.75 $_{PID}$			0.77 $_{PID}$			0.12 $_{PID}$		
ICC	0.84			0.84			0.56		
N	86 $_{PID}$			86 $_{PID}$			86 $_{PID}$		
Observations	172			172			172		
Marginal R^2 / Conditional R^2	0.073 / 0.849			0.073 / 0.853			0.762 / 0.894		

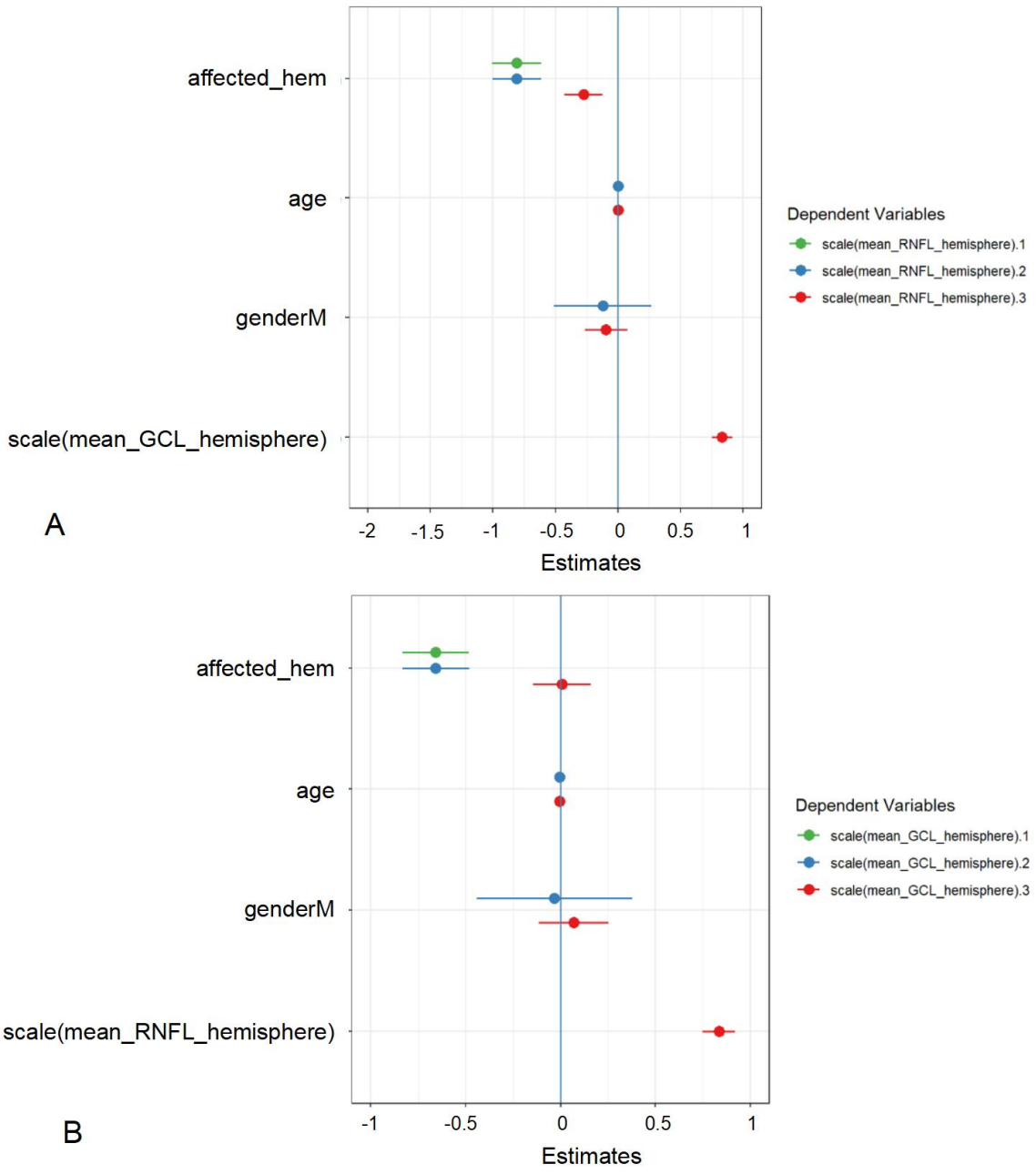

Figure 9: Forest plots illustrating regression estimates for hemispheric differences in RNFL and GCL thickness, corresponding to Table 5A-B. (A) RNFL thickness (dependent variable): affected vs. unaffected hemisphere. (B) GCL thickness (dependent variable): affected vs. unaffected hemisphere. Estimates and 95 % CI are shown for three regression models: univariable (Model 1), adjusted for age and sex (Model 2), and further adjusted for corresponding retinal layer thickness (Model 3). Affected hemisphere remains a consistent predictor of RNFL reduction, while GCL asymmetry is attenuated after full adjustment. CIs crossing zero indicate non-significance.

3.4 Comparison of the rEZR between affected and unaffected hemispheres

To further explore the association between mitochondrial function and glaucomatous damage, inter-hemispheric comparisons of rEZR were conducted across three analytical subgroups.

In the first group, rEZR was compared between the affected and unaffected hemispheres in all participants (57 glaucoma patients and 26 controls), excluding three glaucoma cases with paracentral VF defects. The second analysis focused on glaucoma individuals with a clearly isolated affected hemisphere (n = 35), allowing for more localized comparison of rEZR between hemispheres. In the third group, this comparison was further narrowed to glaucoma patients with isolated hemispheric damage within the significantly affected subgroup (n = 23) (Table 1B).

3.4.1 In all individuals (excluding paracentral defects)

Among all individuals excluding those with paracentral VF defects, no statistically significant difference in rEZR was observed between the affected and unaffected hemispheres. As shown in Figure 5B, NTG cases tended to exhibit lower rEZR values in the affected hemisphere compared to the unaffected side, whereas POAG cases showed no consistent hemispheric asymmetry.

In the univariable model (Table 6A, Model 1), hemisphere status was not significantly associated with rEZR ($p = 0.287$). After adjusting for age and gender (Model 2), age emerged as a significant negative predictor of rEZR ($p = 0.028$), while hemisphere status remained non-significant ($p = 0.227$). In the fully adjusted model (Model 3), which included mean hemispheric GCL and RNFL thickness, the hemispheric difference remained non-significant ($p = 0.857$). In contrast, both age ($p = 0.029$) and gender ($p =$

0.029) were independently associated with rEZR.

These findings are visually confirmed in the forest plot (Figure 10A), where the CIs for hemisphere status consistently cross zero across all models. Collectively, these results suggest that hemispheric difference in rEZR is not detectable at the group level in this cohort, although demographic factors such as age and sex appear to contribute to individual variation.

Table 6: Multivariate linear regression models assessing rEZR differences between affected and unaffected hemispheres. (A) All individuals (excluding paracentral defects). (B) Glaucoma patients with isolated affected hemisphere. (C) Patients in significantly affected group with isolated affected hemisphere. Regression coefficients (Estimates), 95 % CI, and p-values are reported. Statistically significant results ($p < 0.05$) are shown in bold. Model specifications are consistent with previous tables.

A

	Model 1: univariable			Model 2: age & sex adjusted			Model 3: + GCL & RNFL adjusted		
Predictors	*Estimates*	*CI*	*p*	*Estimates*	*CI*	p	Estimates	CI	p
(Intercept)	52.80	48.26 – 57.33	**<0.001**	92.20	61.92 – 122.48	**<0.001**	89.33	59.68 – 118.98	**<0.001**
affected hem	-2.81	-8.01 – 2.39	0.287	-3.17	-8.32 – 1.99	0.227	0.62	-6.14 – 7.38	0.857
age				-0.54	-1.02 – -0.06	**0.028**	-0.53	-1.00 – -0.05	**0.029**
gender [M]				-9.77	-18.06 – -1.48	**0.021**	-9.10	-17.25 – -0.95	**0.029**
mean GCL hemisphere							3.31	-3.13 – 9.74	0.312
mean RNFL hemisphere							0.85	-5.82 – 7.51	0.802
Random Effects									
σ^2	155.08			155.12			159.77		
τ_{00}	272.11 $_{PID}$			241.36 $_{PID}$			222.89 $_{PID}$		
ICC	0.64			0.61			0.58		
N	83 $_{PID}$			83 $_{PID}$			83 $_{PID}$		
Observations	166			166			166		
Marginal R^2 / Conditional R^2	0.004 / 0.639			0.090 / 0.644			0.120 / 0.633		

B

	Model 1: univariable			Model 2: age & sex adjusted			Model 3: + GCL & RNFL adjusted		
Predictors	*Estimates*	*CI*	*p*	*Estimates*	*CI*	p	Estimates	CI	p
(Intercept)	2.71	-6.70 – 12.11	0.562	-15.95	-58.18 – 26.29	0.447	-15.61	-57.61 – 26.38	0.453
affected hem	-0.30	-12.73 – 12.14	0.962	0.47	-11.44 – 12.38	0.936	-2.82	-15.22 – 9.58	0.645
age				0.45	-0.18 – 1.08	0.154	0.50	-0.14 – 1.15	0.123
gender [M]				-13.40	-25.80 – -1.01	**0.035**	-15.67	-28.80 – -2.55	**0.021**
mean GCL global							4.88	-9.22 – 18.99	0.484
mean RNFL global							0.73	-12.58 – 14.05	0.911
Observations	35			35			35		
R^2 / R^2 adjusted	0.000 / -0.030			0.193 / 0.114			0.278 / 0.153		

C

	Model 1: univariable			Model 2: age & sex adjusted			Model 3: + GCL & RNFL adjusted		
Predictors	*Estimates*	*CI*	*p*	*Estimates*	*CI*	p	Estimates	CI	p
(Intercept)	47.90	41.11 – 54.68	**<0.001**	101.97	67.91 – 136.04	**<0.001**	102.14	66.45 – 137.82	**<0.001**
affected hem	-3.40	-10.72 – 3.93	0.355	-3.40	-10.73 – 3.94	0.355	-1.52	-11.50 – 8.46	0.760
age				-0.83	-1.36 – -0.30	**0.003**	-0.85	-1.41 – -0.29	**0.004**
gender [M]				-4.72	-14.90 – 5.46	0.354	-4.41	-15.14 – 6.32	0.411
mean GCL hemisphere							-1.75	-11.00 – 7.49	0.703
mean RNFL hemisphere							3.10	-6.29 – 12.50	0.508
Random Effects									
σ^2	151.64			151.64			150.13		
τ_{00}	108.34 $_{PID}$			56.30 $_{PID}$			69.46 $_{PID}$		
ICC	0.42			0.27			0.32		
N	23 $_{PID}$			23 $_{PID}$			23 $_{PID}$		
Observations	46			46			46		
Marginal R^2 / Conditional R^2	0.011 / 0.423			0.240 / 0.446			0.236 / 0.478		

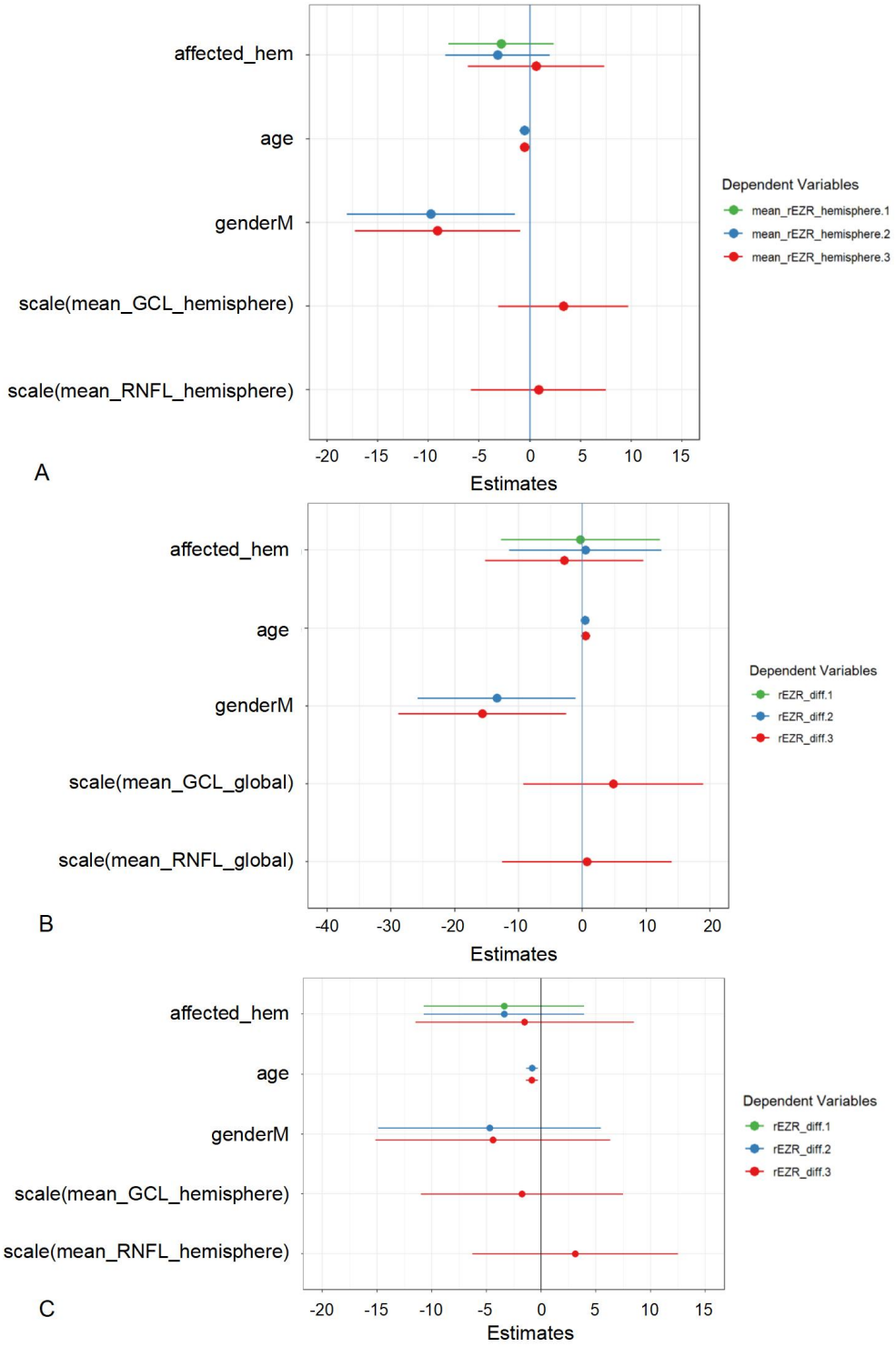

Figure 10: Forest plots illustrating regression estimates for rEZR differences between affected and unaffected hemispheres, corresponding to Table 6A-C. (A) All individuals (excluding paracentral defects). (B) Glaucoma patients with an isolated affected hemisphere. (C) Patients in significantly affected group with an isolated affected hemisphere. Estimates and 95 % CI are shown across models. No significant hemispheric differences in rEZR were observed in any subgroup. Where present, demographic covariates showed associations without altering the primary interpretation.

3.4.2 In glaucoma cases with an isolated affected hemisphere

In glaucoma patients with an isolated hemispheric defect (n = 35), no significant difference in rEZR was observed between affected and unaffected hemispheres. This group included individuals with isolated superior (n = 13), isolated inferior (n = 10), early superior (n = 7), and early inferior (n = 5) field defects (Table 1B).

As shown in Table 6B, the affected hemisphere was not significantly associated with rEZR in any of the models (Model 1: p = 0.962; Model 2: p = 0.936; Model 3: p = 0.645). In contrast, gender emerged as a significant predictor in both adjusted models. In Model 2, male gender was associated with lower rEZR (Estimate = -13.40, 95 % CI: -25.80 to -1.01, p = 0.035), and this association persisted in Model 3 (Estimate = -15.67, 95 % CI: -28.80 to -2.55, p = 0.021). Neither mean global GCL nor RNFL thickness showed significant effects in the final model.

These results are reflected in the forest plot (Figure 10B), where the CIs for hemisphere status intersect zero across all models. In contrast, gender shows a consistent and significant negative association with rEZR in both adjusted models, as indicated by the blue and red lines.

3.4.3 In significantly affected group with an isolated affected hemisphere

Among glaucoma patients in the significantly affected group with an isolated hemispheric defect (n = 23; 13 superior, 10 inferior; see Table 1B), no significant difference in rEZR was observed between affected and unaffected hemispheres.

In univariable analysis (Model 1, Table 6C), hemisphere status was not significantly associated with rEZR (Estimate = -3.40, 95 % CI: -10.72 to 3.93, p = 0.355). This result

remained unchanged after adjusting for age and gender (Model 2), and also after further inclusion of hemispheric GCL and RNFL thickness (Model 3, p = 0.760). Minor associations with age were noted in adjusted models, though these did not alter the overall conclusion.

As shown in the forest plot (Figure 10C), CIs for hemisphere status consistently cross zero across all models, indicating no meaningful hemispheric asymmetry in rEZR in this subgroup.

4. Discussion

In recent years, increasing attention has been directed toward the potential involvement of the outer retinal layer in glaucoma pathophysiology (Chung et al., 2014; Cifuentes-Canorea et al., 2018; Fan et al., 2011; Kita et al., 2016; Unterlauft et al., 2018; Vahedian et al., 2022; Vianna et al., 2019), although this remains a subject of considerable debate. The present study aimed to investigate the relationship between glaucoma and the EZ, a mitochondria-rich region within the inner segments of photoreceptors located in the outer retina. Specifically, we sought to determine whether glaucoma is associated with alterations in rEZR, which may reflect underlying structural or mitochondrial changes, and whether these alterations differ between glaucoma subtypes. By addressing these questions, we hope to provide further evidence linking glaucoma to mitochondrial dysfunction and to explore the potential of rEZR as a novel biomarker for distinguishing between different glaucoma subtypes.

4.1 The Ellipsoid Zone as a Mitochondrial Biomarker in Glaucoma

Mitochondrial dysfunction has been increasingly recognized as a critical contributor to the pathogenesis of glaucoma, particularly in relation to RGCs. Glaucoma shares several pathophysiological features with mitochondrial optic neuropathies, such as Leber’s hereditary optic neuropathy, which is characterized by the selective loss of RGCs (Carelli et al., 2004; Van Bergen et al., 2015). These similarities underscore the hypothesis that glaucoma may, at least in part, be conceptualized as a mitochondriopathy, thereby shifting research focus toward subcellular bioenergetic mechanisms rather than purely mechanical or pressure-related factors.

Visual signal transduction is one of the most energy-intensive processes in the human body. When light enters the eye, it activates photoreceptor cells in the retina, which

transform light signals into electrical impulses that are transmitted through the retinal circuitry to the brain. This complex process is heavily reliant on mitochondrial function to sustain continuous ion transport, neurotransmission, and membrane potential maintenance. Within the retina, photoreceptors, RPE, and RGCs are particularly enriched with mitochondria, making them especially sensitive to metabolic stress (Carrella et al., 2021).

Among these, the EZ represents a mitochondria-dense substructure within the inner segments of photoreceptors and appears as a distinct hyperreflective band in OCT imaging. Due to its high mitochondrial content, the EZ serves as an indirect optical marker of photoreceptor metabolic integrity. Previous studies have reported outer retinal involvement in glaucoma, including reductions in cone photoreceptor density (Nork et al., 2000; Panda and Jonas 1992), suggesting that mitochondrial stress in photoreceptors may occur under glaucomatous conditions.

Given that the EZ reflects mitochondrial density and organization, alterations in its reflectivity - quantified as the rEZR - may serve as a non-invasive biomarker for assessing mitochondrial function in vivo. This is particularly relevant considering that glaucoma is increasingly being understood not only as an optic neuropathy but also as a neurodegenerative disorder with mitochondrial underpinnings.

Furthermore, differences in clinical features and pathophysiological mechanisms between POAG and NTG raise the possibility of subtype-specific patterns of mitochondrial vulnerability. While POAG is primarily associated with elevated IOP, NTG is more often linked to systemic vascular dysregulation, impaired ocular blood flow, and nocturnal hypotension (Lešták et al., 2019). These differences may result in distinct mitochondrial stress profiles across glaucoma subtypes. Therefore, investigating rEZR in both POAG and NTG may not only enhance our understanding of glaucoma

pathogenesis but also support the development of precision biomarkers for subtype differentiation and individualized disease management.

4.2 Moving from Limited to Localized: Enhancing EZ Detection through Volumetric and Hemispheric Mapping

Previous studies, such as those by Ha et al., demonstrated that the EZ intensity decreases in glaucoma patients with IOP ≤ 21 mmHg, based on horizontal and vertical single-line scans across the fovea (Ha et al., 2018; Ha et al., 2019). Moreover, reductions in EZ intensity appeared to increase with disease progression. While these findings highlight a potential association between glaucoma and EZ alterations, the methodological limitations of single-line scanning must be acknowledged.

Given the well-established anatomical organization of RGC axons - converging in a highly structured pattern toward the optic nerve head - glaucomatous damage typically manifests in localized regions, especially during early stages. This leads to characteristic VF defects, such as nasal steps and arcuate scotomas (Jansonius et al., 2009). Such spatial specificity limits the sensitivity of single-line scans in detecting regionally distributed EZ alterations, particularly outside the central fovea.

Additionally, NTG is believed to be more susceptible to vascular dysregulation and impaired ocular perfusion, which may be influenced by systemic factors such as nocturnal hypotension, sleep apnea, and peripheral vascular dysregulation. These conditions raise the possibility that mitochondrial stress in outer retinal photoreceptors could be more pronounced in NTG than in other glaucoma subtypes. Although elevated IOP is a well-established risk factor in glaucoma, its direct impact on mitochondrial function within photoreceptors remains poorly understood. It is therefore plausible that mitochondrial vulnerability and stress responses differ between POAG and NTG,

warranting further subtype-specific comparative investigation.

To address these limitations, the present study employed volumetric macular scanning to enhance sensitivity in detecting mitochondrial alterations within the EZ. We compared the rEZR across POAG, NTG, and healthy controls. Furthermore, to account for the anatomical course of RGC axon bundles and the known hemispheric asymmetry of glaucomatous damage, the macular volume was divided into superior and inferior hemispheres, symmetrically aligned along the fovea–disc axis. This hemisphere-specific mapping approach was designed to detect localized EZ changes that may be overlooked by single-line scanning techniques, particularly in early-stage disease or spatially selective damage patterns.

4.3 Mechanistic Insights into the Absence of EZ Alterations in Glaucoma

In this section, we examine potential mechanisms underlying the absence of significant quantitative changes in EZ reflectivity, as measured by rEZR, in patients with POAG and NTG. Although mitochondrial dysfunction is a well-established contributor to glaucomatous neurodegeneration, particularly affecting RGCs, our findings suggest that the outer retinal photoreceptors appear structurally preserved - at least insofar as can be inferred from OCT-based reflectivity analysis. Several mechanisms may account for this observation, including differences in metabolic demands between RGCs and photoreceptors, protective features of the outer retinal vascular supply, and the limited susceptibility of photoreceptors to retrograde transsynaptic degeneration.

4.3.1 Metabolic Resilience of Photoreceptors Compared to RGCs

One plausible explanation for the preserved EZ reflectivity in glaucoma lies in the fundamental differences in energy metabolism between RGCs and photoreceptors. A

growing body of evidence suggests that mitochondrial dysfunction plays a key role in glaucomatous neurodegeneration, particularly in relation to RGCs (Ju et al., 2023; Liu et al., 2020; Lo Faro et al., 2021; Osborne 2008). In the DBA/2J (D2) mouse model of glaucoma, Williams et al. used electron microscopy to demonstrate mitochondrial abnormalities specifically in RGC dendrites, characterized by reduced cristae volume - a feature absent in normal controls (Williams et al., 2017). These findings highlight the metabolic vulnerability of RGCs under glaucomatous stress.

RGCs rely predominantly on mitochondrial oxidative phosphorylation for ATP generation, particularly within their unmyelinated axons and dendrites, which have high energy demands due to active signal transmission and synaptic integration. Each compartment of the RGC - dendrites, soma, axon hillock, and distal axon - has distinct energetic profiles and mitochondrial densities (Yu et al., 2013). Importantly, their metabolic activity is highly compartmentalized and less buffered by glial or vascular support, making them sensitive to localized energy deficits. Differences in axonal length and myelination status also influence mitochondrial distribution and ATP availability, potentially contributing to the different rates of RGC death observed in POAG (Osborne 2010). Overall, this structural and bioenergetic specialization renders RGCs particularly susceptible to mitochondrial stress and ATP depletion (Lee et al., 2011).

In contrast, photoreceptors exhibit robust and spatially concentrated mitochondrial populations, especially within the EZ, to sustain their high energy requirements for phototransduction (Fu et al., 2019). They represent the most numerous retinal neurons, comprising approximately 60 % of the total neuronal population (Li et al., 2015). While photoreceptors are also highly energy-demanding, their metabolic strategies differ fundamentally from those of RGCs. Despite abundant mitochondrial content, photoreceptors preferentially utilize aerobic glycolysis producing lactate even under normoxic conditions (Brown et al., 2019; Hurley 2021). This lactate is not simply a waste

product; rather, it is efficiently recycled by adjacent RPE cells and Müller glial cells, which convert it into oxidative substrates that support ATP generation via mitochondrial respiration (Kanow et al., 2017).

Moreover, photoreceptors retain the capacity to utilize alternative energy sources, such as fatty acid β-oxidation, which can be activated under conditions of metabolic stress or glucose scarcity (Fu et al., 2021). Their close anatomical and metabolic coupling with RPE cells further enhances resilience by supporting nutrient transport, redox homeostasis, and mitochondrial substrate exchange. Importantly, the metabolic network surrounding photoreceptors provides both metabolic redundancy and intercellular metabolic support - particularly through tightly coordinated interactions with the RPE - which together buffer against localized mitochondrial dysfunction and confer greater resilience compared to RGCs. This metabolic robustness may partly explain why rEZR remained stable in our study, even in glaucoma patients with advanced structural damage to the inner retina, as evidenced by significant thinning of both the RNFL and the GCL.

4.3.2 Choroidal Circulation and the Ischemic Resilience of the Outer Retina

Another plausible explanation for the preservation of EZ reflectivity in glaucoma lies in the distinct vascular supply of the retina, which creates differential susceptibility to ischemic injury between the inner and outer retinal layers. The inner retina is perfused by the central retinal artery, whereas the outer retina - including the photoreceptors, RPE, outer nuclear layer, and outer plexiform layer - receives its blood supply exclusively from the choroidal circulation (Pournaras et al., 2008). These two vascular systems are not only anatomically separate but also differ markedly in their structural and physiological characteristics.

Capillaries of the central retinal artery form the inner blood–retinal barrier through tight endothelial junctions, functionally similar to the blood–brain barrier. In contrast, choroidal capillaries are fenestrated and have polarized endothelium, allowing for a greater rate of oxygen and nutrient exchange (Bernstein and Hollenberg 1965; Pournaras et al., 2008). These structural differences give rise to distinct hemodynamic characteristics: the inner retinal circulation is tightly autoregulated and relatively low-flow, whereas the choroidal circulation is high-flow and low-resistance, but with limited autoregulatory capacity (Kur et al., 2012). This divergence in vascular architecture and control contributes to the differential responses of the inner and outer retina to ocular perfusion changes, particularly in their vulnerability to ischemic injury.

According to the vascular theory of glaucomatous optic neuropathy, insufficient ocular blood flow - whether resulting from elevated IOP, systemic hypotension, or vascular dysregulation - can lead to localized ischemia and progressive neurodegeneration (Flammer 1994; Flammer et al., 2002). A key physiological determinant of ocular blood flow is ocular perfusion pressure (OPP), which is defined as the difference between mean arterial pressure and IOP.

The inner retina, supplied by the central retinal artery, exhibits strong autoregulatory capacity, allowing blood flow to remain relatively stable during moderate OPP fluctuations (Kur et al., 2012; Riva et al., 1981). However, it operates under a low-flow, high-oxygen extraction system - akin to that of cerebral circulation - and is therefore highly dependent on uninterrupted perfusion (Flammer et al., 2002). RGCs, consume substantial amounts of oxygen to support synaptic signaling and are highly sensitive to hypoxia (Kergoat et al., 2006), rendering them especially vulnerable to sustained or severe reductions in OPP (Chidlow et al., 2017). Furthermore, stoichiometric analyses have demonstrated that RGCs consume at least five times more oxygen than photoreceptors to sustain visual processing (Noell 1951), underscoring their greater vulnerability to hypoxic stress.

By contrast, the outer retina is supplied by the choroidal circulation, which lacks significant autoregulatory control (Linsenmeier and Zhang 2017). Nevertheless, its exceptionally high basal blood flow and diffusional oxygen delivery help maintain photoreceptor oxygenation under moderate hypoperfusion (Alm and Bill 1972; Wangsa-Wirawan and Linsenmeier 2003). Hypoxic challenges are known to preferentially affect the inner retinal layers, while the outer retina exhibits relative resistance to oxygen deprivation (Janáky et al., 2007; Tinjust et al., 2002). This physiological resilience is partly attributable to the anatomical and vascular organization of the outer retina. Due to the relatively long diffusion distance from the choriocapillaris to the photoreceptor inner segments, a steep oxygen gradient across the RPE and Bruch's membrane is required to sustain oxidative metabolism. To support this gradient, the choroid must preserve a high local PO_2, which in turn necessitates a high-flow, low-oxygen extraction vascular system (Linsenmeier and Padnick-Silver 2000). This vascular system not only ensures adequate oxygen delivery under normal conditions but also confers a buffering capacity against transient reductions in OPP (Alm and Bill 1972; Nickla and Wallman 2010). Experimental studies support this distinction. Transient ischemic events frequently cause infarction of the inner retinal layers, while photoreceptors can often survive prolonged ischemia and recover function upon reperfusion (Hayreh 2004; Hughes 1991; Zhao et al., 2013). This resilience may be attributed to specialized metabolic adaptations, efficient utilization of substrates in the subretinal space, or other protective mechanisms that are not yet fully understood (Casson et al., 2021).

This combination of structural, vascular, and metabolic advantages may underlie the preservation of EZ integrity observed in our study, even in eyes exhibiting significant damage to the inner retina.

4.3.3 Limited Transsynaptic Degeneration in Photoreceptors

A third potential explanation for the preserved EZ reflectivity in glaucoma is the limited involvement of photoreceptors in retrograde transsynaptic degeneration (RTSD) following RGC loss. RTSD refers to the process by which damage propagates upstream from injured postsynaptic neurons to their presynaptic partners. In both humans and animal models, RTSD of RGCs has been well documented following occipital lobe lesions, indicating that the retina is capable of undergoing retrograde degeneration along the visual pathway (Beatty et al., 1982; Haddock and Berlin 1950; Vanburen 1963).

Several studies have suggested that glaucoma may induce secondary changes in the outer retina (Choi et al., 2011; Fan et al., 2011; Hasegawa et al., 2015; Kendell et al., 1995; Nork et al., 2000; Werner et al., 2011), potentially mediated by transsynaptic mechanisms. Bipolar cells relay visual signals from photoreceptors and horizontal cells to RGCs, either directly or indirectly through amacrine cells. Since transneuronal degeneration can occur in both retrograde and anterograde directions (Jindahra et al., 2009), it is theoretically possible that RGC loss in glaucoma could lead to structural or functional alterations in upstream neurons, including photoreceptors.

However, the evidence supporting photoreceptor involvement in glaucomatous RTSD remains limited and inconclusive. RTSD is known to be a slow process, often taking years to manifest observable changes (Jindahra et al., 2012). Recent in vivo imaging studies have provided compelling evidence that cone photoreceptors remain structurally intact in glaucomatous eyes, even in regions with long-standing VF loss and thinning of the RNFL. For example, Hasegawa et al. used adaptive optics scanning laser ophthalmoscopy and SD-OCT to examine cone photoreceptors in areas corresponding to VF defects of at least three years' duration (Hasegawa et al., 2016). Their findings demonstrated preserved cone structure despite substantial RGC damage.

Similar results were obtained in a porcine model of optic nerve injury. Komáromy et al. performed unilateral RGC axotomy in domestic pigs and observed no evidence of retrograde transsynaptic degeneration in the outer retina even nine months after surgery (Komáromy et al., 2003). Given the anatomical and physiological similarity between porcine and human retinas, these results support the notion that RTSD may have a limited effect on photoreceptors in glaucomatous optic neuropathy.

These converging lines of evidence indicate that retrograde transsynaptic degeneration is unlikely to significantly compromise photoreceptor integrity in glaucoma. This may help explain why EZ reflectivity, as measured by rEZR, remained unaltered in our study despite substantial RGC and RNFL damage.

4.4 Interpretation of RNFL and GCL Findings in Glaucoma

Consistent with previous studies (Unterlauft et al., 2018), our results revealed significant thinning of both the RNFL and GCL in regions corresponding to VF defects, indicating RNFL and RGC damage. These findings support the view that while inner retinal structures are compromised in glaucoma, photoreceptors may remain unaffected.
In our hemisphere-specific analysis (Model 3), we compared RNFL and GCL thickness between affected and unaffected hemispheres. The results showed that RNFL thinning was significant in the hemisphere with VF loss, whereas GCL thickness did not show a statistically significant difference. Furthermore, the mean RNFL thickness in the affected hemisphere emerged as a strong predictor of glaucomatous damage (Estimate = 0.84, $p < 0.001$). This suggests that structural changes in the GCL may be, at least in part, secondary to or dependent on preceding RNFL alterations, reflecting the anatomical and functional relationship between these two retinal layers.

The observed dissociation between RNFL and GCL alterations aligns with previous

reports indicating that RNFL thickness is a more sensitive indicator of early glaucomatous damage than GCL thickness (Choi et al., 2017; Miraftabi et al., 2016). In early glaucoma, axonal loss often precedes detectable changes in the ganglion cell soma, particularly within the macular region. As a result, localized RNFL thinning may occur without concurrent or measurable GCL changes.

Anatomically, the highest density of RGCs is concentrated within ± 8 degrees of the foveal center, a region comprising less than 2 % of the total retinal area but containing over 30 % of all RGCs (Curcio and Allen 1990). Building upon this spatial organization, Hood and colleagues developed a schematic model that identifies distinct regions of glaucomatous vulnerability based on the anatomical distribution of RGC axons and their corresponding retinal projections (Hood 2017; Hood et al., 2013). Within this framework, three zones are particularly relevant: the superior vulnerability zone (SVZ), the inferior vulnerability zone (IVZ), and the macular vulnerability zone (MVZ) (Figure 11). The SVZ and IVZ are two arcuate sectors on the optic disc that are most susceptible to early glaucomatous damage, corresponding to the superior-temporal and inferior-temporal sectors, respectively. These regions primarily reflect damage to arcuate nerve fiber bundles originating from the peripheral macula and adjacent retinal areas. The MVZ, on the other hand, is a distinct subregion located within the temporal portion of the IVZ. It overlaps directly with the inferior macula and is strongly associated with glaucomatous damage due to its inclusion of axons from the most densely packed central RGCs. While the SVZ does not overlap with the central macula, the IVZ does, making the MVZ a critical site for detecting changes within the macular region. This anatomical framework helps explain why RNFL and GCL measurements may show spatially discordant patterns of damage in glaucoma. RNFL thinning, which reflects axonal loss along arcuate bundles, is often observed in the SVZ and IVZ, including areas beyond the central macula. In contrast, GCL thickness measurements are typically derived from macular-centered scans and are most sensitive to changes within the MVZ. As a result, glaucomatous

damage occurring in peripheral regions may be captured by RNFL assessments but missed by GCL-based analyses. Hood further noted that RNFL damage at retinal locations outside the central ± 8° zone does not always correspond to abnormalities in

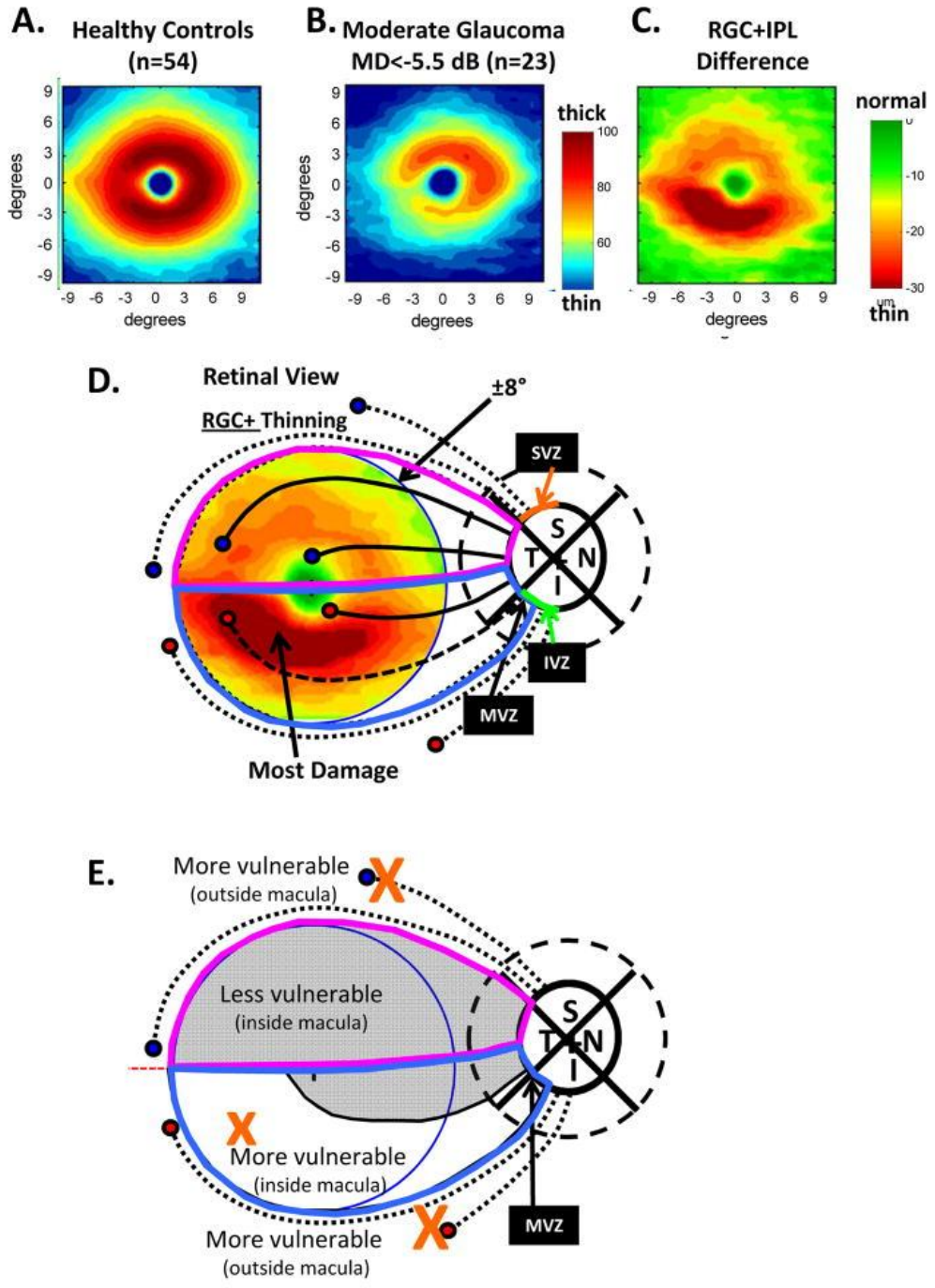

Figure 11: RGC plus inner plexiform thickness (RGC+) and glaucomatous damage seen with SD-OCT. Reprinted from (Hood 2017), Prog Retin Eye Res, 57:46-75. https://doi.org/10.1016/j.preteyeres.2016.12.002. © 2017 Elsevier. Reproduced with permission. (A) The

average RGC+ thickness map for 54 healthy controls shown in pseudo-color. (B) The average RGC+ thickness map for 23 patients with moderate glaucoma (i.e., 24-2 VF mean deviation (MD) worse than −5.5 dB) shown in pseudo-color. (C) A difference map generated by subtracting the RGC+ thickness map for the age-similar controls in panel A from the RGC+ thickness map in panel C. The color indicates the degree of thinning. (D) The schematic model of the macula is superimposed upon the central ± 8° of panel C to indicate the relationship of the thinned region in panel C to the region projecting to the MVZ. The circles represent groups of RGCs and the associated black lines bundles of axons. The axon bundles with solid black lines feed into the temporal quadrant, while those with the interrupted black lines project to the SVZ (upper dotted), the MVZ of the IVZ (dashed) and IVZ outside the MVZ (lower dotted). (E) The regions from panel D are shown with the more and less vulnerable regions labelled.

GCL probability maps. This reinforces the importance of interpreting RNFL and GCL data in tandem and recognizing the spatial limitations of each layer's diagnostic utility.

Therefore, the dissociation between RNFL and GCL thinning underscores the value of comprehensive inner retinal layer assessment in glaucoma. Particular attention should be paid to RNFL alterations in anatomically vulnerable regions, even when corresponding GCL changes are not yet apparent on structural OCT.

4.5 Methodological Advances and Research Implications

This study is the first to utilize a semi-automated analysis system based on mitochondrial imaging biomarkers to investigate outer retinal mitochondrial changes in patients with different subtypes of glaucoma. By leveraging high-resolution volumetric scanning and analyzing the rEZR, we were able to achieve a more comprehensive and spatially detailed assessment of mitochondrial integrity compared to previous studies that relied primarily on single-line scans. The macula-centered volume scan was symmetrically aligned with the fovea–disc axis, following the anatomical distribution of the RNFL, thereby enhancing the anatomical relevance and spatial resolution of the analysis.

These methodological advances not only provide novel clinical evidence for understanding the relationship between glaucoma and photoreceptor mitochondrial

integrity but also offer new research strategies for exploring retinal biomarkers. This work thus lays a foundation for future studies into mitochondrial dysfunction in glaucoma and contributes to the refinement of imaging-based biomarker development. Nevertheless, despite these strengths, several methodological and analytical limitations should be acknowledged.

4.6 Study Limitations

This study has several limitations that should be considered when interpreting the findings. (1) The sample size was relatively small, comprising only 60 glaucoma participants, which may have reduced the statistical power of the analyses and increased the likelihood of overlooking true differences - that is, failing to detect actual effects that do exist. (2) Although the quantification of rEZR was performed using an automated algorithm, the overall process remained semi-automated due to the need for manual correction of retinal layer segmentation. Given that each eye was scanned using 241 B-scans, the procedure was time-consuming and required a high degree of patient cooperation. This was particularly challenging for elderly individuals or those with unstable fixation, dry eye, or other ocular surface conditions, which may have introduced artifacts or segmentation errors that reduced the accuracy of rEZR measurements. (3) The inclusion of a substantial proportion of early and pre-perimetric glaucoma cases (accounting for nearly half of the glaucoma group) may have limited our ability to detect changes in photoreceptor mitochondria. Since both transsynaptic degeneration and photoreceptor structural alterations are believed to develop gradually over time, mitochondrial impairment may only become apparent in more advanced stages (Abu-Amero et al., 2006; Lee et al., 2012). It is also known that when there is a VF defect manifestation, the RGC loss reaches about 30 % (Kerrigan-Baumrind et al., 2000). Therefore, future studies may benefit from focusing on patients with late-stage glaucoma, where mitochondrial dysfunction is likely to be more pronounced. (4) The IOP thresholds

used to define POAG and NTG subgroups were relatively broad. Applying stricter classification criteria, such as a peak IOP greater than 24 mmHg for POAG (as 24 mmHg represents the treatment threshold for ocular hypertension (National Institute for Health and Care Excellence, 2019)) and a peak IOP less than 16 mmHg for NTG (a value proposed as a more stringent benchmark for IOP-lowering success), may help improve diagnostic clarity and better distinguish pressure-related differences in mitochondrial stress. The optic nerve head is known to have a high mitochondrial density and to depend heavily on mitochondrial function. When IOP increases, retinal ganglion cells are particularly vulnerable to metabolic failure (Barron et al., 2004), suggesting that IOP-induced mitochondrial dysfunction warrants further investigation. (5) Our analysis divided the macular volume into only two hemispheric regions (superior and inferior), which may have limited the ability to capture spatially localized changes in rEZR. Incorporating both structural (RNFL and GCL) and functional (VF sensitivity) data may enable a more targeted and meaningful regional analysis. (6) Although age and gender were identified as statistically significant predictors in some regression models, their effect sizes were small and inconsistent. These associations are more likely to reflect sample variability or residual confounding than genuine biological relevance. To validate or refute these weak associations, future studies should include larger, more demographically diverse cohorts and apply more comprehensive adjustments for clinical covariates such as systemic vascular conditions (e.g., hypertension, diabetes), glaucoma treatment history, and other systemic or ocular factors that may influence mitochondrial function or retinal reflectivity measures.

5. Summary

In conclusion, this study found no significant reduction in EZ reflectivity on SD-OCT in either POAG or NTG patients, even in retinal regions with marked thinning of the RNFL and GCL. These findings suggest that photoreceptor mitochondria may remain structurally intact despite glaucomatous damage to inner retinal layers. Although growing evidence implicates mitochondrial dysfunction in the pathogenesis of glaucoma, its direct impact on outer retinal photoreceptors remains uncertain. It is possible that glaucoma exerts minimal influence on photoreceptor mitochondria, or that current imaging techniques lack the sensitivity to detect subtle mitochondrial alterations over the course of disease progression. Nevertheless, the EZ represents a promising structural marker for probing mitochondrial health in the retina. Future research should focus on the development of more advanced imaging tools and the identification of sensitive biomarkers to further elucidate the role of mitochondria in glaucomatous neurodegeneration. This work lays a foundation for future longitudinal and mechanistic studies focused on mitochondrial biomarkers and their diagnostic potential in glaucoma subtyping and monitoring.

6. List of figures

7. List of tables

8. Reference

Abu-Amero KK, Morales J and Bosley TM. Mitochondrial abnormalities in patients with primary open-angle glaucoma. Invest Ophthalmol Vis Sci. 2006. 47: 2533-2541

Alm A and Bill A. The oxygen supply to the retina. II. Effects of high intraocular pressure and of increased arterial carbon dioxide tension on uveal and retinal blood flow in cats. A study with radioactively labelled microspheres including flow determinations in brain and some other tissues. Acta Physiol Scand. 1972. 84: 306-319

Barbosa-Breda J, Van Keer K, Abegão-Pinto L, Nassiri V, Molenberghs G, Willekens K, Vandewalle E, Rocha-Sousa A and Stalmans I. Improved discrimination between normal-tension and primary open-angle glaucoma with advanced vascular examinations - the Leuven Eye Study. Acta Ophthalmol. 2019. 97: e50-e56

Barron MJ, Griffiths P, Turnbull DM, Bates D and Nichols P. The distributions of mitochondria and sodium channels reflect the specific energy requirements and conduction properties of the human optic nerve head. Br J Ophthalmol. 2004. 88: 286-290

Bartoń K (2025). MuMIn: Multi-Model Inference. R package version 1.48.11. https://CRAN.R-project.org/package=MuMIn (Accessed: 06.05.2025)

Bates D, Mächler M, Bolker B and Walker S. Fitting Linear Mixed-Effects Models Using lme4. Journal of Statistical Software. 2015. 67: 1 - 48

Beatty RM, Sadun AA, Smith L, Vonsattel JP and Richardson EP, Jr. Direct demonstration of transsynaptic degeneration in the human visual system: a comparison of retrograde and anterograde changes. J Neurol Neurosurg Psychiatry. 1982. 45: 143-146

Bernstein MH and Hollenberg MJ. Fine structure of the choriocappillaris and retinal capillaries. Invest Ophthalmol. 1965. 4: 1016-1025

Brown EE, DeWeerd AJ, Ildefonso CJ, Lewin AS and Ash JD. Mitochondrial oxidative stress in the retinal pigment epithelium (RPE) led to metabolic dysfunction in both the RPE and retinal photoreceptors. Redox Biol. 2019. 24: 101201

Carelli V, Ross-Cisneros FN and Sadun AA. Mitochondrial dysfunction as a cause of optic neuropathies. Prog Retin Eye Res. 2004. 23: 53-89

Carrella S, Massa F and Indrieri A. The Role of MicroRNAs in Mitochondria-Mediated Eye Diseases. Front Cell Dev Biol. 2021. 9: 653522

Casson RJ, Chidlow G, Crowston JG, Williams PA and Wood JPM. Retinal energy metabolism in health and glaucoma. Prog Retin Eye Res. 2021. 81: 100881

Chidlow G, Wood JPM and Casson RJ. Investigations into Hypoxia and Oxidative Stress at the Optic Nerve Head in a Rat Model of Glaucoma. Front Neurosci. 2017. 11: 478

Choi JA, Shin HY, Park HL and Park CK. The Pattern of Retinal Nerve Fiber Layer and Macular Ganglion Cell-Inner Plexiform Layer Thickness Changes in Glaucoma. J Ophthalmol. 2017. 2017: 6078365

Choi SS, Zawadzki RJ, Lim MC, Brandt JD, Keltner JL, Doble N and Werner JS. Evidence of outer retinal changes in glaucoma patients as revealed by ultrahigh-resolution in vivo retinal imaging. Br J Ophthalmol. 2011. 95: 131-141

Chung HS, Sung KR, Lee KS, Lee JR and Kim S. Relationship between the lamina cribrosa, outer retina, and choroidal thickness as assessed using spectral domain optical coherence tomography. Korean J Ophthalmol. 2014. 28: 234-240

Cifuentes-Canorea P, Ruiz-Medrano J, Gutierrez-Bonet R, Peña-Garcia P, Saenz-Frances F, Garcia-Feijoo J and Martinez-de-la-Casa JM. Analysis of inner and

outer retinal layers using spectral domain optical coherence tomography automated segmentation software in ocular hypertensive and glaucoma patients. PLoS One. 2018. 13: e0196112

Curcio CA and Allen KA. Topography of ganglion cells in human retina. J Comp Neurol. 1990. 300: 5-25

Drance S, Anderson DR and Schulzer M. Risk factors for progression of visual field abnormalities in normal-tension glaucoma. Am J Ophthalmol. 2001. 131: 699-708

Duarte JN. Neuroinflammatory Mechanisms of Mitochondrial Dysfunction and Neurodegeneration in Glaucoma. J Ophthalmol. 2021. 2021: 4581909

Fan N, Huang N, Lam DS and Leung CK. Measurement of photoreceptor layer in glaucoma: a spectral-domain optical coherence tomography study. J Ophthalmol. 2011. 2011: 264803

Flammer J. The vascular concept of glaucoma. Surv Ophthalmol. 1994. 38 Suppl: S3-6

Flammer J, Orgül S, Costa VP, Orzalesi N, Krieglstein GK, Serra LM, Renard JP and Stefánsson E. The impact of ocular blood flow in glaucoma. Prog Retin Eye Res. 2002. 21: 359-393

Fu Z, Chen CT, Cagnone G, Heckel E, Sun Y, Cakir B, Tomita Y, Huang S, Li Q, Britton W, Cho SS, Kern TS, Hellström A, Joyal JS and Smith LE. Dyslipidemia in retinal metabolic disorders. EMBO Mol Med. 2019. 11: e10473

Fu Z, Kern TS, Hellström A and Smith LEH. Fatty acid oxidation and photoreceptor metabolic needs. J Lipid Res. 2021. 62: 100035

Ha A, Kim YK, Jeoung JW and Park KH. Ellipsoid Zone Change According to Glaucoma Stage Advancement. Am J Ophthalmol. 2018. 192: 1-9

Ha A, Sun S, Kim YK, Jeoung JW, Kim HC and Park KH. Automated Quantification of Macular Ellipsoid Zone Intensity in Glaucoma Patients: the Method and its Comparison with Manual Quantification. Sci Rep. 2019. 9: 19771

Haddock JN and Berlin L. Transsynaptic degeneration in the visual system; report of a case. Arch Neurol Psychiatry. 1950. 64: 66-73

Hasegawa T, Akagi T, Yoshikawa M, Suda K, Yamada H, Kimura Y, Nakanishi H, Miyake M, Unoki N, Ikeda HO and Yoshimura N. Microcystic Inner Nuclear Layer Changes and Retinal Nerve Fiber Layer Defects in Eyes with Glaucoma. PLoS One. 2015. 10: e0130175

Hasegawa T, Ooto S, Takayama K, Makiyama Y, Akagi T, Ikeda HO, Nakanishi H, Suda K, Yamada H, Uji A and Yoshimura N. Cone Integrity in Glaucoma: An Adaptive-Optics Scanning Laser Ophthalmoscopy Study. Am J Ophthalmol. 2016. 171: 53-66

Hayreh SS. Posterior ciliary artery circulation in health and disease: the Weisenfeld lecture. Invest Ophthalmol Vis Sci. 2004. 45: 749-757; 748

Hood DC. Improving our understanding, and detection, of glaucomatous damage: An approach based upon optical coherence tomography (OCT). Prog Retin Eye Res. 2017. 57: 46-75

Hood DC, Raza AS, de Moraes CG, Liebmann JM and Ritch R. Glaucomatous damage of the macula. Prog Retin Eye Res. 2013. 32: 1-21

Hughes WF. Quantitation of ischemic damage in the rat retina. Exp Eye Res. 1991. 53: 573-582

Hurley JB. Retina Metabolism and Metabolism in the Pigmented Epithelium: A Busy Intersection. Annu Rev Vis Sci. 2021. 7: 665-692

Janáky M, Grósz A, Tóth E, Benedek K and Benedek G. Hypobaric hypoxia reduces the amplitude of oscillatory potentials in the human ERG. Doc Ophthalmol. 2007. 114: 45-51

Jansonius NM, Nevalainen J, Selig B, Zangwill LM, Sample PA, Budde WM, Jonas JB, Lagrèze WA, Airaksinen PJ, Vonthein R, Levin LA, Paetzold J and Schiefer U. A mathematical description of nerve fiber bundle trajectories and their variability in the human retina. Vision Res. 2009. 49: 2157-2163

Jeoung JW, Seong MW, Park SS, Kim DM, Kim SH and Park KH. Mitochondrial DNA variant discovery in normal-tension glaucoma patients by next-generation sequencing. Invest Ophthalmol Vis Sci. 2014. 55: 986-992

Jindahra P, Petrie A and Plant GT. Retrograde trans-synaptic retinal ganglion cell loss identified by optical coherence tomography. Brain. 2009. 132: 628-634

Jindahra P, Petrie A and Plant GT. The time course of retrograde trans-synaptic degeneration following occipital lobe damage in humans. Brain. 2012. 135: 534-541

Ju WK, Perkins GA, Kim KY, Bastola T, Choi WY and Choi SH. Glaucomatous optic neuropathy: Mitochondrial dynamics, dysfunction and protection in retinal ganglion cells. Prog Retin Eye Res. 2023. 95: 101136

Kanow MA, Giarmarco MM, Jankowski CS, Tsantilas K, Engel AL, Du J, Linton JD, Farnsworth CC, Sloat SR, Rountree A, Sweet IR, Lindsay KJ, Parker ED, Brockerhoff SE, Sadilek M, Chao JR and Hurley JB. Biochemical adaptations of the retina and retinal pigment epithelium support a metabolic ecosystem in the vertebrate eye. Elife. 2017. 6:

Kendell KR, Quigley HA, Kerrigan LA, Pease ME and Quigley EN. Primary open-angle glaucoma is not associated with photoreceptor loss. Invest Ophthalmol Vis Sci. 1995. 36: 200-205

Kergoat H, Hérard ME and Lemay M. RGC sensitivity to mild systemic hypoxia. Invest Ophthalmol Vis Sci. 2006. 47: 5423-5427

Kerrigan-Baumrind LA, Quigley HA, Pease ME, Kerrigan DF and Mitchell RS. Number of ganglion cells in glaucoma eyes compared with threshold visual field tests in the same persons. Invest Ophthalmol Vis Sci. 2000. 41: 741-748

Kita Y, Anraku A, Kita R and Goldberg I. The clinical utility of measuring the macular outer retinal thickness in patients with glaucoma. Eur J Ophthalmol. 2016. 26: 118-123

Komáromy AM, Brooks DE, Källberg ME, Dawson WW, Szél A, Lukáts A, Samuelson DA, Sapp HL, Jr., Gelatt KN and Sherwood MB. Long-term effect of retinal ganglion cell axotomy on the histomorphometry of other cells in the porcine retina. J Glaucoma. 2003. 12: 307-315

Kur J, Newman EA and Chan-Ling T. Cellular and physiological mechanisms underlying blood flow regulation in the retina and choroid in health and disease. Prog Retin Eye Res. 2012. 31: 377-406

Kuznetsova A, Brockhoff PB and Christensen RHB. lmerTest Package: Tests in Linear Mixed Effects Models. Journal of Statistical Software. 2017. 82: 1 - 26

Lee S, Sheck L, Crowston JG, Van Bergen NJ, O'Neill EC, O'Hare F, Kong YX, Chrysostomou V, Vincent AL and Trounce IA. Impaired complex-I-linked respiration and ATP synthesis in primary open-angle glaucoma patient lymphoblasts. Invest Ophthalmol Vis Sci. 2012. 53: 2431-2437

Lee S, Van Bergen NJ, Kong GY, Chrysostomou V, Waugh HS, O'Neill EC, Crowston JG and Trounce IA. Mitochondrial dysfunction in glaucoma and emerging bioenergetic therapies. Exp Eye Res. 2011. 93: 204-212

Leske MC, Wu SY, Hennis A, Honkanen R and Nemesure B. Risk factors for incident open-angle glaucoma: the Barbados Eye Studies. Ophthalmology. 2008. 115: 85-93

Lešták J, Pitrová Š, Nutterová E and Bartošová L. Normal tension vs high tension glaucoma: an - overview. Cesk Slov Oftalmol. 2019. 75: 55-60

Li L, Anand M, Rao KN and Khanna H. Cilia in photoreceptors. Methods Cell Biol. 2015. 127: 75-92

Linsenmeier RA and Padnick-Silver L. Metabolic dependence of photoreceptors on the choroid in the normal and detached retina. Invest Ophthalmol Vis Sci. 2000. 41: 3117-3123

Linsenmeier RA and Zhang HF. Retinal oxygen: from animals to humans. Prog Retin Eye Res. 2017. 58: 115-151

Liu H, Mercieca K and Prokosch V. Mitochondrial Markers in Aging and Primary Open-Angle Glaucoma. J Glaucoma. 2020. 29: 295-303

Lo Faro V, Nolte IM, Ten Brink JB, Snieder H, Jansonius NM and Bergen AA. Mitochondrial Genome Study Identifies Association Between Primary Open-Angle Glaucoma and Variants in MT-CYB, MT-ND4 Genes and Haplogroups. Front Genet. 2021. 12: 781189

Miraftabi A, Amini N, Morales E, Henry S, Yu F, Afifi A, Coleman AL, Caprioli J and Nouri-Mahdavi K. Macular SD-OCT Outcome Measures: Comparison of Local Structure-Function Relationships and Dynamic Range. Invest Ophthalmol Vis Sci. 2016. 57: 4815-4823

Mwanza JC, Oakley JD, Budenz DL, Chang RT, Knight OJ and Feuer WJ. Macular ganglion cell-inner plexiform layer: automated detection and thickness reproducibility with spectral domain-optical coherence tomography in glaucoma. Invest Ophthalmol Vis Sci. 2011. 52: 8323-8329

National Institute for Health and Care Excellence (NICE) (2019). Exceptional surveillance of glaucoma: diagnosis and management (NICE guideline NG81). In: National Institute for Health and Care Excellence Guidelines. London: NICE. https://www.nice.org.uk/guidance/ng81 (Accessed: 20.03.2024)

Nickla DL and Wallman J. The multifunctional choroid. Prog Retin Eye Res. 2010. 29: 144-168

Noell WK. Site of asphyxial block in mammalian retinae. J Appl Physiol. 1951. 3: 489-500

Nork TM, Ver Hoeve JN, Poulsen GL, Nickells RW, Davis MD, Weber AJ, Vaegan, Sarks SH, Lemley HL and Millecchia LL. Swelling and loss of photoreceptors in chronic human and experimental glaucomas. Arch Ophthalmol. 2000. 118: 235-245

Osborne NN. Mitochondria: Their role in ganglion cell death and survival in primary open angle glaucoma. Exp Eye Res. 2010. 90: 750-757

Osborne NN. Pathogenesis of ganglion "cell death" in glaucoma and neuroprotection: focus on ganglion cell axonal mitochondria. Prog Brain Res. 2008. 173: 339-352

Osborne NN and del Olmo-Aguado S. Maintenance of retinal ganglion cell mitochondrial functions as a neuroprotective strategy in glaucoma. Curr Opin Pharmacol. 2013. 13: 16-22

Panda S and Jonas JB. Decreased photoreceptor count in human eyes with secondary angle-closure glaucoma. Invest Ophthalmol Vis Sci. 1992. 33: 2532-2536

Pournaras CJ, Rungger-Brändle E, Riva CE, Hardarson SH and Stefansson E. Regulation of retinal blood flow in health and disease. Prog Retin Eye Res. 2008. 27: 284-330

Quigley HA. Glaucoma. Lancet. 2011. 377: 1367-1377

Quigley HA and Broman AT. The number of people with glaucoma worldwide in 2010 and 2020. Br J Ophthalmol. 2006. 90: 262-267

R Core Team (2020). R: A language and environment for statistical computing. Vienna: R Foundation for Statistical Computing. https://www.R-project.org/ (Accessed: 20.03.2024)

Riva CE, Sinclair SH and Grunwald JE. Autoregulation of retinal circulation in response to decrease of perfusion pressure. Invest Ophthalmol Vis Sci. 1981. 21: 34-38

Sakurada Y, Mabuchi F and Kashiwagi K. Genetics of primary open-angle glaucoma and its endophenotypes. Prog Brain Res. 2020. 256: 31-47

Shin HJ, Lee SH, Chung H and Kim HC. Association between photoreceptor integrity and visual outcome in diabetic macular edema. Graefes Arch Clin Exp Ophthalmol. 2012. 250: 61-70

Spaide RF and Curcio CA. Anatomical correlates to the bands seen in the outer retina by optical coherence tomography: literature review and model. Retina. 2011. 31: 1609-1619

Tham YC, Li X, Wong TY, Quigley HA, Aung T and Cheng CY. Global prevalence of glaucoma and projections of glaucoma burden through 2040: a systematic review and meta-analysis. Ophthalmology. 2014. 121: 2081-2090

Thiele S, Isselmann B, Pfau M, Holz FG, Schmitz-Valckenberg S, Wu Z, Guymer RH and Luu CD. Validation of an Automated Quantification of Relative Ellipsoid Zone Reflectivity on Spectral Domain-Optical Coherence Tomography Images. Transl Vis Sci Technol. 2020. 9: 17

Tinjust D, Kergoat H and Lovasik JV. Neuroretinal function during mild systemic hypoxia. Aviat Space Environ Med. 2002. 73: 1189-1194

Trivli A, Koliarakis I, Terzidou C, Goulielmos GN, Siganos CS, Spandidos DA, Dalianis G and Detorakis ET. Normal-tension glaucoma: Pathogenesis and genetics. Exp Ther Med. 2019. 17: 563-574

Unterlauft JD, Rehak M, Böhm MRR and Rauscher FG. Analyzing the impact of glaucoma on the macular architecture using spectral-domain optical coherence tomography. PLoS One. 2018. 13: e0209610

Vahedian Z, Fakhraie G, Ghasemi M, Azimi A and Tabatabaei SM. The thickness of the outer retina in the macula and circumpapillary area in patients with unilateral advanced glaucoma. Graefes Arch Clin Exp Ophthalmol. 2022. 260: 3935-3944

Van Bergen NJ, Crowston JG, Craig JE, Burdon KP, Kearns LS, Sharma S, Hewitt AW, Mackey DA and Trounce IA. Measurement of Systemic Mitochondrial Function in Advanced Primary Open-Angle Glaucoma and Leber Hereditary Optic Neuropathy. PLoS One. 2015. 10: e0140919

Vanburen JM. TRANS-SYNAPTIC RETROGRADE DEGENERATION IN THE VISUAL SYSTEM OF PRIMATES. J Neurol Neurosurg Psychiatry. 1963. 26: 402-409

Vianna JR, Butty Z, Torres LA, Sharpe GP, Hutchison DM, Shuba LM, Nicolela MT and Chauhan BC. Outer retinal layer thickness in patients with glaucoma with horizontal hemifield visual field defects. Br J Ophthalmol. 2019. 103: 1217-1222

Wangsa-Wirawan ND and Linsenmeier RA. Retinal oxygen: fundamental and clinical aspects. Arch Ophthalmol. 2003. 121: 547-557

Weinreb RN and Khaw PT. Primary open-angle glaucoma. Lancet. 2004. 363: 1711-1720

Werner JS, Keltner JL, Zawadzki RJ and Choi SS. Outer retinal abnormalities associated with inner retinal pathology in nonglaucomatous and glaucomatous optic neuropathies. Eye (Lond). 2011. 25: 279-289

Williams PA, Harder JM, Foxworth NE, Cardozo BH, Cochran KE and John SWM. Nicotinamide and WLD(S) Act Together to Prevent Neurodegeneration in Glaucoma. Front Neurosci. 2017. 11: 232

Yang XJ, Ge J and Zhuo YH. Role of mitochondria in the pathogenesis and treatment of glaucoma. Chin Med J (Engl). 2013. 126: 4358-4365

Yu DY, Cringle SJ, Balaratnasingam C, Morgan WH, Yu PK and Su EN. Retinal ganglion cells: Energetics, compartmentation, axonal transport, cytoskeletons and vulnerability. Prog Retin Eye Res. 2013. 36: 217-246

Zhao Y, Yu B, Xiang YH, Han XJ, Xu Y, So KF, Xu AD and Ruan YW. Changes in retinal morphology, electroretinogram and visual behavior after transient global ischemia in adult rats. PLoS One. 2013. 8: e65555

9. Declaration of Personal Contribution

This dissertation was conducted at the Department of Ophthalmology, University of Bonn, under the official supervision of Prof. Dr. med. Frank G. Holz. I would like to thank him for supporting this doctoral project and enabling my research within the department. The scientific supervision and day-to-day guidance were provided by Priv.-Doz. Dr. Karl Mercieca, who closely mentored me throughout the project. The concept and design of the study were developed by myself in collaboration with Priv.-Doz. Dr. Karl Mercieca and Priv.-Doz. Dr. med. Sarah Thiele. I was responsible for patient recruitment, conducting ophthalmological examinations, and processing image data. I also contributed to the data analysis. Priv.-Doz. Dr. Karl Mercieca provided scientific guidance throughout the research process. The statistical analysis of the data was carried out by Dr. Leonie Weinhold (affiliated with the Institute for Medical Biometry, Informatics and Epidemiology - IMBIE) and Ben Isselmann. The section on statistical analysis within the dissertation was written by myself with support from Dr. Benjamin Aretz (also affiliated with IMBIE). Dr. med. Leonie Bourauel reviewed the manuscript and provided valuable comments and suggestions for improvement. The writing of the dissertation, including the structuring, interpretation of results, and integration of all sections, was carried out independently by myself.

I hereby declare that I have written this dissertation independently and have not used any sources or aids other than those indicated by me.

10. Acknowledgements

First and foremost, I would like to express my sincere gratitude to Prof. Dr. med. Frank G. Holz and Priv.-Doz. Dr. Karl Mercieca for giving me the opportunity to pursue my doctoral studies at the Department of Ophthalmology, University of Bonn. Their support has been instrumental in allowing me to carry out this research in such a stimulating academic environment.

I am especially thankful to Priv.-Doz. Dr. Karl Mercieca for his invaluable guidance, encouragement, and continuous supervision throughout the entire course of my doctoral research. His expertise and constructive feedback have played a crucial role in shaping the scientific quality of this dissertation.

I would also like to thank Priv.-Doz. Dr. med. Sarah Thiele for her insightful input and collaborative spirit in the early stages of study planning, and Dr. med. Leonie Bourauel for her thoughtful review and helpful suggestions on the manuscript.

I gratefully acknowledge the contributions of Dr. Leonie Weinhold and Ben Isselmann, who performed the statistical analysis, as well as Dr. Benjamin Aretz for his kind assistance in interpreting the statistical methods.

I also extend my appreciation to the entire team at the Department of Ophthalmology for their collegial support, and to all patients who participated in the study, without whom this research would not have been possible.

Lastly, I would like to thank my family and friends for their constant encouragement, patience, and emotional support throughout this journey.